

Hurricane Gustav (2008) Waves and Storm Surge: Hindcast, Synoptic Analysis and Validation in Southern Louisiana

J.C. Dietrich^{1,+,*}, J.J. Westerink¹, A.B. Kennedy¹, J.M. Smith², R.E. Jensen²,
M. Zijlema³, L.H. Holthuijsen³, C. Dawson⁴, R.A. Luetlich Jr.⁵,
M.D. Powell⁶, V.J. Cardone⁷, A.T. Cox⁷, G.W. Stone⁸, H. Pourtaheri⁹,
M.E. Hope¹, S. Tanaka¹, L.G. Westerink¹, H.J. Westerink¹, Z. Cobell^{1,++}

¹ Department of Civil Engineering and Geological Sciences, University of Notre Dame

² Coastal and Hydraulics Laboratory, U.S. Army Engineer Research and Development Center

³ Faculty of Civil Engineering and Geosciences, Delft University of Technology

⁴ Institute for Computational Engineering and Sciences, University of Texas at Austin

⁵ Institute of Marine Sciences, University of North Carolina at Chapel Hill

⁶ Atlantic Oceanographic and Meteorological Labs, Hurricane Research Division, NOAA

⁷ Oceanweather Inc

⁸ Coastal Studies Institute, Louisiana State University

⁹ New Orleans District, U.S. Army Corps of Engineers

⁺ Currently: Institute for Computational Engineering and Sciences, University of Texas at Austin

⁺⁺ Currently: Arcadis Inc., Denver, Colorado

* Corresponding author: dietrich@ices.utexas.edu

Institute for Computational Engineering and Sciences, University of Texas at Austin

1 University Station, C0200, Austin, TX, 78712

Monthly Weather Review

Submitted on August 19, 2010

In revised form on January 18, 2011

In re-revised form on March 4, 2011

Version 086, last modified by jcd

Abstract

Hurricane Gustav (2008) made landfall in southern Louisiana on 1 September 2008 with its eye never closer than 75km to New Orleans, but its waves and storm surge threatened to flood the city. Easterly tropical-storm-strength winds impacted the region east of the Mississippi River for 12-15hr, allowing for early surge to develop up to 3.5m there and enter the river and the city's navigation canals. During landfall, winds shifted from easterly to southerly, resulting in late surge development and propagation over more than 70km of marshes on the river's west bank, over more than 40km of Caernarvon Marsh on the east bank, and into Lake Pontchartrain to the north. Wind waves with estimated significant heights of 15m developed in the deep Gulf of Mexico but were reduced in size once they reached the continental shelf. The barrier islands further dissipated the waves, and locally-generated seas existed behind these effective breaking zones.

The hardening and innovative deployment of gages since Hurricane Katrina (2005) resulted in a wealth of measured data for Gustav. A total of 39 wind wave time histories, 362 water level time histories, and 82 high water marks were available to describe the event. Computational models, including the structured-mesh WAM and STWAVE wave models and the unstructured-mesh SWAN wave and ADCIRC circulation models, resolve the region with unprecedented levels of detail, with an unstructured-mesh spacing of 100-200m in the wave-breaking zones and 20-50m in the small-scale channels. Data-assimilated winds were applied using H*Wind and IOKA procedures. Wave and surge computations from these models are validated comprehensively at the measurement locations ranging from the deep Gulf of Mexico, along the coast and into the rivers and floodplains of southern Louisiana and are described and quantified within context of the evolution of the storm.

1. Introduction

New Orleans and its infrastructure are surrounded by extensive levees and raised features, marshes to the south and east, and barrier islands on the Louisiana-Mississippi shelf. Hurricane Katrina (2005) exposed vulnerabilities as it generated storm surge throughout the region, flooding in the city due to breaches along its shipping and drainage canals, and water levels along the Mississippi coastline that were the largest measured in the United States (Ebersole *et al.*, 2007). But Katrina was an especially large and devastating hurricane. It reached Category 5 on the Saffir-Simpson Scale in the Gulf of Mexico before weakening to Category 3 prior to its first landfall, maintained its intensity through the Breton and Chandeleur Sounds, and tracked near metropolitan New Orleans (Knabb *et al.*, 2005).

Hurricane Gustav (2008) was the first major hurricane to track through southeast Louisiana since Katrina (Figure 1), and it made landfall on 1 September 2008. Gustav was much weaker than Katrina, both in the Gulf and at landfall, it tracked farther west, and its eye was never closer than 75km to New Orleans. For those reasons, its waves and surge were expected to be less threatening to the city. However, Gustav increased in size as it approached Louisiana, and its outer, tropical-storm-strength winds impacted the system for 12-15hr. Gustav generated waves that damaged infrastructure in southern Louisiana and offshore, and its surge nearly overtopped large sections of the levee/floodwall system throughout metropolitan New Orleans.

Measured data for waves and surge are more extensive and detailed than for any previous Gulf hurricane. Measured time series describe wave generation, propagation, and dissipation from the deep Gulf of Mexico onto the continental shelf and into the marshes and coastal floodplains. The National Data Buoy Center (NDBC) collected measurements at its buoys throughout the Gulf, where the depths range to several kilometers and the peak wave heights

reached an estimated 15m. On the shelf, the Coastal Studies Institute (CSI, <http://www.wavcis.lsu.edu>) collected measurements at five stations west of the Mississippi River delta, where a decrease in bathymetry and wave damping limited the peak wave heights to 3-5m. Sixteen gages deployed by Andrew Kennedy (AK) of the University of Notre Dame were located along the coastline from Calcasieu Pass to Pensacola Bay, in depths ranging from 1-20m, and they offer an unprecedented description of the nearshore wave behavior during a major hurricane (Kennedy *et al.*, 2010). Additionally, six gages deployed by the Coastal Hydraulics Laboratory (CHL) of the US Army Engineer Research and Development Center (USA-ERDC) show the dissipation of waves in the Terrebonne and Biloxi marshes. This level of available wave data was possible due to permanent gage hardening and the increased deployment of temporary gages since Katrina.

High-water marks (HWMs) were collected by the Federal Emergency Management Agency (FEMA), while time series of water levels were collected by AK, CHL, the US Army Corps of Engineers (USACE), the US Geological Survey (USGS), the National Oceanic and Atmospheric Administration (NOAA), and the Coastwide Reference Monitoring System (CRMS). These data show how the surge evolved throughout the storm. Water levels are reported relative to the North American Vertical Datum of 1988 (NAVD88) updated to the 2004.65 epoch, unless otherwise noted. Surge of 2.5-3m was pushed across the shelf and against the levees of lower Plaquemines Parish, which is fronted by a relatively narrow marsh and Breton Sound. The river levees extend farther southward on the west bank, and they helped to capture and steer this surge upriver. Surge accumulated against the levees near the confluence of the Gulf Intracoastal Waterway (GIWW) and the Mississippi River Gulf Outlet (MRGO), where it flowed into the Inner Harbor Navigation Canal (IHNC) and the center of the city, reaching to

3.5m. There were reports of wave overtopping of the city floodwalls and levees (Figure 2a), although no breaches occurred. An early set-up of 1m along the southwest shore of Lake Pontchartrain became 2-2.25m after the lake filled. To the east of the river, the surge reached 2.5m against the levees near English Turn and Braithwaite (Figure 2b), which are fronted by 40km of Caernarvon Marsh that marginally attenuated the water levels. To the west of the river, a surge of 2-2.5m developed near Port Fourchon and Grand Isle as the storm was making landfall. When the winds shifted, surge was pushed into Terrebonne and Barataria Bays, northward through the interconnected marshes and waterways, and reached 1m near the west bank of New Orleans, but not until 12-36hr after landfall. Thus, despite making landfall more than 75km from New Orleans, Gustav created significant surge on all sides of the city.

Due to the complexities of southern Louisiana and its response to hurricane forcing, computational models have been developed that utilize unstructured meshes to resolve at basin, shelf, floodplain and channel scales (Westerink *et al.*, 2008; Bunya *et al.*, 2010). Mesh resolution varies from kilometers in deep water to tens of meters in the small-scale channels and features inland and near the levee protection system. These meshes incorporate the frictional dissipation due to variability in land cover, local geology and bottom sediments (Bunya *et al.*, 2010; Sheremet and Stone, 2003). Surge is allowed to propagate onto the continental shelf and interact with the complex geometry and land cover nearshore and inland. The ADvanced CIRCulation (ADCIRC) shallow-water model was validated on the unstructured SL15 mesh for Hurricanes Katrina and Rita (2005), and it showed high levels of model skill for tides, riverine stages, waves and storm surge (Bunya *et al.*, 2010; Dietrich *et al.*, 2010). The SL15 model was used extensively for design work and analysis by the USACE, FEMA and local agencies (Ebersole *et al.*, 2007; FEMA, 2009a; USACE, 2009).

The Gustav hindcast utilizes the latest SL16 mesh, which contains twice the resolution of the SL15 mesh. The Gulf is resolved with resolution of 4-6km, and the mesh size decreases accordingly on the shelf to 500-1000m. In the wave breaking zones and inland, the resolution is never greater than 200m, to improve the wave breaking and the transfer of wave radiation stress gradients to ADCIRC. In the small-scale channels and passes, such as the Mississippi River and its distributaries, the MRGO, and the Rigolets and Chef Menteur passes, the resolution varies to 20-50m. Bathymetry and topography were re-applied from the latest sources, as described below.

Advancements have also been made in the coupling of wave and circulation models. ADCIRC has been coupled to two structured-mesh wave models: the deepwater WAVE Model (WAM) on a basin scale, and the nearshore STEADY-state WAVE (STWAVE) model on regional scales (Komen *et al.*, 1994; Smith, 2000; Smith *et al.*, 2001; Günther, 2005; Bunya *et al.*, 2010; Dietrich *et al.*, 2010). The spectral wave energy from WAM was interpolated and used as boundary conditions for five nearshore STWAVE meshes, four of which allowed waves to propagate only in the half plane directed onshore. Now STWAVE has been applied with full-plane propagation in all nearshore meshes. Alternatively, ADCIRC has been coupled with the unstructured-mesh version of the Simulating WAVES Nearshore (SWAN) model (SiadatMousavi *et al.*, 2009; Zijlema, 2010). SWAN+ADCIRC employs the same unstructured mesh on the same computational cores, passing information between models through local memory/cache, and thus it can simulate the propagation of waves from deep water to the nearshore with accuracy and efficiency (Dietrich *et al.*, 2011).

These new models are well-positioned to simulate hurricanes in southern Louisiana, and Gustav is an appropriate validation test because of its size and track, the quality of data-

assimilated wind fields available to force models, and the wealth of measured waves and water levels. A total of 39 wind wave time histories, 362 water level time histories, and 82 HWMs were available to describe the event. In the sections that follow, we describe the models and characterize the system, discuss how the storm evolved and impacted the region, and perform a detailed validation of these coupled wave and surge model hindcasts using the measured time series of waves and water levels as well as HWMs.

2. SL16 Model Development

a. Hurricane Wind Field

Hurricane wind fields for Gustav were developed using NOAA's Hurricane Research Division Wind Analysis System (H*Wind) to assimilate winds in the core from extensive aircraft, buoy, space-based remote sensing, wind-tower and other measurement data (Powell *et al.*, 1996; 1998; 2010). H*Wind analyses of Gustav benefited from the deployment of Stepped-Frequency Microwave Radiometers aboard the Air Force Hurricane Hunter Aircraft (Uhlhorn *et al.*, 2007), increasing the availability of high radial resolution surface winds since the Katrina wind field post-analysis (Ebersole *et al.*, 2007). Additional improvements to the H*Wind analysis included the use of improved terrain conversions (Vickery *et al.*, 2009) and high-resolution tower data from Texas Tech University and the Florida Coastal Monitoring Program. H*Wind analyses cover an 8° latitude-longitude domain on a 3hr frequency for Gustav's entire Gulf track. To provide forcing to our wave and circulation models, the H*Wind fields are blended with larger scale winds using the Interactive Objective Kinematic Analysis (IOKA) system (Cox *et al.*, 1995; Cardone and Cox, 2007). The resulting wind fields apply to the reference condition of 10m height, 30min "sustained" wind speed and marine exposure. Wind fields were interpolated to 15min intervals, starting at 0000 UTC 26 August 2008 (approximately

6.5 days before landfall) and ending at 0000 UTC 04 September 2008 (approximately 2.5 days after landfall). The Gustav wind fields offer Gulf-wide resolution on a 0.05° mesh, with increased resolution of 0.015° on a smaller mesh near landfall.

These resulting wind fields and Holland (1980) model-generated pressure fields are read and interpolated by ADCIRC onto its unstructured mesh and then passed to the wave models. ADCIRC applies a factor of 1.09 to convert from 30min-averaged to 10min-averaged wind speeds, and directional wind reduction factors are applied (Bunya *et al.*, 2010). In addition, ADCIRC applies a wind drag coefficient based on recent analyses of the azimuthal dependence of the drag coefficient determined from mean GPS sonde wind speed profiles (Powell *et al.*, 2003; Powell, 2006). Data were inconclusive to determine whether an azimuthal drag dependence exists for near coastal areas. However, for the results based primarily on open-ocean, deepwater wind profiles, the drag coefficient increases in sectors where the winds are blowing across or counter in direction to the waves. ADCIRC detects the location and direction of the eye, and then the sector-based wind drag coefficients are applied as shown in Figure 3. These wind drag coefficients are shared with SWAN.

WAM utilizes an atmospheric input source term based on Janssen (1991) that includes the net impact surface roughness resulting from a growing wave field, with an upper limit where the dependency of frictional velocity becomes linear with the equivalent neutral stable marine exposure wind field at 10m. STWAVE applies a drag coefficient consistent with Cardone (1969).

b. Wave and Surge Models

The coupling of ADCIRC and STWAVE is performed through external files. WAM is run first, on a Gulf-wide mesh with fixed 0.05° resolution, to generate boundary conditions at the

nearshore, structured STWAVE meshes (Komen *et al.*, 1994; Smith, 2000; Smith *et al.*, 2001; Günther, 2005; Smith, 2007). WAM is a third-generation, discrete spectral wave model solving the action balance equation (including refraction and shoaling) and accounting for arbitrary water depth in source/sink term specification to compute the generation and dissipation of wave action. It uses 28 frequency bins that increase in bandwidth logarithmically, and 24 directional bins of constant width 15° . ADCIRC is then run, and its wind fields and water levels are output to use as forcing for a set of STWAVE simulations on two nearshore meshes with 200m resolution. STWAVE solves the action balance equation along piecewise, backward-traced wave rays. STWAVE utilizes 45 frequency bins, on the range 0.0314-2.08Hz and increasing in bandwidth logarithmically ($\Delta\sigma/\sigma \approx 0.1$), and 72 directional bins of constant width 5° . This coupling provides good matches for nearshore waves and storm surge, and a realistic wave set-up (Bunya *et al.*, 2010; Dietrich *et al.*, 2010).

In the coupling of SWAN+ADCIRC, the unstructured-mesh version of SWAN is applied so that both models run on the same mesh, thus eliminating the need for interpolation between models (Zijlema, 2010; Dietrich *et al.*, 2011). Water levels and currents are computed by ADCIRC and passed at each SWAN time step. SWAN solves the action balance equation for the wave action (Booij *et al.*, 1999; Ris *et al.*, 1999). The SWAN time step and coupling interval are 600s (Dietrich *et al.*, 2011). The wave directions are discretized into 36 directional bins of constant width 10° , and the frequencies are discretized over 40 bins on a logarithmic scale, over the range 0.031-1.42Hz. The hindcast uses the wind input formulation based on Snyder *et al.* (1981), the modified whitecapping expression of Rogers *et al.* (2003), and quadruplet nonlinear interactions via the Discrete Interaction Approximation (Hasselmann *et al.*, 1985). For the shallow-water source terms, depth-induced breaking is computed with a spectral version of the

model due to Battjes and Janssen (1978) with the breaking index $\gamma = 0.73$; bottom friction is described below. Wave refraction is enabled in regions where the resolution of the bathymetry is sufficient to prevent spurious wave refraction over one spatial element, specifically in the northern Gulf.

ADCIRC solves the 2D and 3D shallow-water equations for water levels ζ and the vertically-integrated momentum equations for currents U and V (Kolar *et al.*, 1994; Luettich and Westerink, 2004; Dawson *et al.*, 2006). The depth-averaged 2D equations are employed herein because there is significant, wave-induced vertical mixing on the continental shelf. The unstructured mesh allows for resolution to increase as waves and surge propagate from the deeper Gulf to the continental shelf and into the inlets and floodplains of coastal regions. ADCIRC uses a 1s time step in the present hindcast.

c. SL16 Unstructured Mesh

This study employs the high-resolution SL16 mesh, which has 5,035,113 vertices and 9,945,623 triangular elements. As shown in Figure 4-5, the mesh provides coverage of southern Louisiana, Mississippi and Alabama, and it extends outward through the Gulf of Mexico and the Caribbean Sea to the western North Atlantic Ocean. This wide coverage allows tides to be specified at a boundary outside the resonant basin of the Gulf, and storms to be started inside the domain but far from the area of interest. The mesh resolution varies from 15-20km in the Atlantic Ocean, to 4-6km in the Gulf, to 1km on the continental shelf and, as highlighted in Figure 6, to 100-200m in the wave-breaking zones and marshes of southern Louisiana, and to 20-50m in small-scale channels.

Bathymetry in the Gulf was specified using the 1 arc-minute global relief model ETOPO1 in deep water (Amante and Eakins, 2009) and Coastal Relief DEMs nearshore (NOAA,

2008). Bathymetry in nearshore water bodies and channels, such as the Mississippi River, Lakes Borgne and Pontchartrain, and the Rigolets and Chef Menteur passes, was applied from recent surveys by the USACE and NOAA. Topography in the marshes was specified based on the land cover databases described below, while topography farther inland was specified using LiDAR (<http://atlas.lsu.edu/lidar/>). These bathymetric/topographic data were applied via mesh-scale averaging to avoid irregularities or discontinuities in the SL16 mesh. Levee and road systems that are barriers to flood propagation are included, with geographical placement based on USACE surveys and heights from USACE or LiDAR; these levees are handled as lines of vertices or sub-mesh-scale weirs (Westerink *et al.*, 2008). Levee and road heights were established to reflect pre-Gustav conditions.

d. Adjustments for Steric Expansion and Vertical Datum

Water levels are increased at the beginning of the ADCIRC simulation to account for the vertical datum and the intra-annual mean sea surface variability of the Gulf of Mexico. The computed water levels in ADCIRC are relative to local mean sea level, and they are adjusted to the North American Vertical Datum of 1988 updated to the 2004.65 epoch, NAVD88 (2004.65), by adding 0.134m (Garster *et al.*, 2007; Bunya *et al.*, 2010). A further adjustment is required because of the intra-annual fluctuation in sea level due to the thermal expansion of the Gulf and other processes. Long-term NOAA stations at Dauphin Island, MS, and Grand Isle and Eugene Island, LA, indicate a steric increase of 0.086m in the averaged water levels in early September (<http://tidesandcurrents.noaa.gov/sltrends/sltrends.html>). Thus the combined increase in water levels for Gustav is $0.134\text{m} + 0.086\text{m} = 0.22\text{m}$.

e. Integrally-Coupled Bottom Friction

Hydraulic friction is computed in ADCIRC using a Manning's n formulation (Figure 7), with spatially-variable values that are applied based on land-cover databases (Bunya *et al.*, 2010), specifically data from the Louisiana Gap Analysis Program (LA-GAP, <http://atlas.lsu.edu/rasterdown.htm>), the Mississippi Gap Analysis Program (MS-GAP, <http://www.basic.ncsu.edu/segap/index.html>) and the Coastal Change Analysis Program (C-CAP, <http://www.csc.noaa.gov/digitalcoast/data/ccapregional/>). These values are summarized in Table 2-4. On the continental shelf in the Gulf of Mexico, the values have been set to $n = 0.022$ for sand/gravel bottoms, and $n = 0.012$ for muddy bottoms, such as the LA-MS continental shelf (Buczowski *et al.*, 2006). These values also enable the currents and geostrophic set-up associated with the forerunner surge in Hurricane Ike (Kennedy *et al.*, 2011).

STWAVE applies bottom friction based on the same Manning's n values used by ADCIRC (Smith, 2007), but with a minimum of $n \geq 0.03$. In addition, the integrated coupling of SWAN+ADCIRC allows for friction to be adjusted during the simulation, based on the computed solution of the model components. This hindcast utilizes the formulation of Madsen *et al.* (1988), who employ a roughness length z_o , which is expressed in terms of the water depth H and the Manning's n :

$$z_o = H \exp \left[- \left(1 + \frac{\kappa H^{1/6}}{n \sqrt{g}} \right) \right],$$

where $\kappa = 0.4$ is the von Karman constant, and g is the gravitational acceleration (Bretschneider *et al.*, 1986). New roughness lengths are computed at each SWAN time step, based on the computed ADCIRC water depth and Manning's n value at each mesh vertex. The Manning's n

values are raised to $n \geq 0.03$ to prevent the use of unrealistically small roughness lengths in SWAN; the values remain unchanged for ADCIRC.

f. Riverine Inflows

River inflows are specified for the Mississippi and Atchafalaya Rivers at Baton Rouge and Simmesport, LA, respectively, using a river-wave radiation boundary condition (Westerink et al., 2008; Bunya *et al.*, 2010). A steady flow boundary condition is applied during a 0.5day hyperbolic ramp, and then the river is allowed to reach equilibrium over the next 3.5days. After four days of simulation, the boundary condition is switched to a wave radiation boundary condition, and tide, wind, pressure and wind wave forcings are applied throughout the system. River flow rates were determined from the New Orleans District of the US Army Corps of Engineers (<http://www.mvn.usace.army.mil>), and were applied as average values during the seven days surrounding landfall. The flow rates were $8,920\text{m}^3\text{s}^{-1}$ and $3,823\text{m}^3\text{s}^{-1}$ for the Mississippi and Atchafalaya Rivers, respectively.

3. Measured Time Series and High-Water Marks

Gustav is characterized by measurement data that describe how the storm evolved as it traversed the Gulf and made landfall in southeast Louisiana. More permanent gages survived Gustav than Katrina, partly due to efforts to harden the gages and increase their reliability. Additional gages were deployed before landfall, in regions such as the marshes and nearshore that have been under-represented. The following sections describe the measurement data, which offer valuable descriptions of the hurricane behavior in those regions, and which provide excellent validation data for WAM, STWAVE, SWAN and ADCIRC.

a. NDBC Waves

The NDBC operates discus buoys throughout the Gulf; they have diameters that range from 3m nearshore to 10-12m in the deeper Gulf. They measure heave acceleration or vertical displacement, which are processed both on the buoy and then onshore to derive spectral wave energies, which are integrated to derive wave properties such as significant height, peak and mean period, and mean direction (<http://www.ndbc.noaa.gov/>). These measured wave properties are compared to modeled results from WAM, STWAVE and SWAN at 12 NDBC buoys within the Gulf.

b. CSI Waves and Water Levels

The CSI at Louisiana State University operates stations along the continental shelf offshore of Louisiana. Each station utilizes a digiquartz pressure transducer and a Marsh-McBirney current meter at depths of 1-2m below mean sea level, and these measurements are processed to derive water depths and directional wave spectra (WAVCIS, <http://www.wavcis.lsu.edu/>). The measured significant wave heights, peak periods and water levels are compared to modeled results from STWAVE, SWAN and ADCIRC at five stations located along the south-central Louisiana coast between the Vermilion and Barataria Bays. The water depths are converted to water levels by subtracting the mean depth at each station and accounting for the steric expansion and datum adjustment to NAVD88 (2004.65).

c. AK Waves and Water Levels

The AK gages measured waves and water levels using bottom-mounted pressure sensors recording continuously at 1Hz (Kennedy *et al.*, 2010). These gages were deployed over two days pre-landfall using helicopters, and were retrieved using boats and divers post-storm.

Measured absolute pressures were converted to water depths using records of atmospheric pressure. Surge elevations were then computed as the low-pass filtered water levels, while significant wave heights were computed using standard spectral methods, corrected using computed depth-averaged currents. The measured significant wave heights, peak periods, and water levels are compared to modeled results from STWAVE, SWAN and ADCIRC at 16 gages located along the coastline from Calcasieu Pass in the west to Pensacola Bay in the east.

d. CHL Waves and Water Levels

CHL deployed three bottom-mounted pressure gauges in Biloxi Marsh and three in Terrebonne Marsh in depths of 0.5-1.2m (Smith *et al.*, 2011). The gages were YSI 600XLM pressure gages, and they were sampled hourly at 2Hz. Analysis of the inner marsh gages resulted in peak periods around 2s (0.5Hz) at the peak of the storm, which was near the high-frequency cut-off for the spectral analysis. This can result in amplification of noise and either over- or under-estimation of wave height and under-estimation of wave period.

e. NOAA Water Levels

NOAA operates tide measurement stations along the coastline of the United States (<http://www.tidesandcurrents.noaa.gov/>). The measured water levels are compared to modeled results from ADCIRC at 23 stations along the coastline from Naples, FL, to Vermilion Bay. The measured water levels are relative to NAVD88 (2004.65).

f. USACE Water Levels

The USACE operates pressure gauges throughout southern Louisiana, and a total of 42 gages produced time series of water levels during part or all of Gustav. These data were

obtained from the New Orleans District (USACE-MVN), and these water levels are relative to NAVD88 (2004.65).

g. USGS Water Levels

The USGS operates pressure gages throughout southern Louisiana, and a total of 18 gages produced time series of water levels during Gustav (Walters, 2009). Most of the gages provide water levels relative to NAVD88 (2004.65), but a few gages near the Terrebonne and Barataria Bays were reported relative to NGVD29. In addition, the USGS deployed 24 pressure gages during Gustav that also produced time series of water levels during all or part of Gustav (Walters, 2009). These measured water levels are all relative to NAVD88 (2004.65).

h. CRMS High-Water Marks

The Coastwide Reference Monitoring System (CRMS, <http://www.lacoast.gov/crms2/home.aspx>) is a joint effort by federal and Louisiana state agencies to collect data about water quality. The gages provide water levels relative to NAVD88 (2004.65). The data set was trimmed to 232 gages by removing gages whose records were incomplete or otherwise were limited near the peak of the storm, and also the gages with obvious datum inconsistencies. The peak hydrograph values at the 232 gages are compared to modeled results from ADCIRC.

i. FEMA High-Water Marks

Finally, FEMA (2009b) measured HWMs relative to NAVD88 (2004.65) throughout southern Louisiana. These HWMs were collected in mid-November 2008, more than two months after Gustav made landfall, and thus they contain contributions from Hurricane Ike as well. The measured HWMs are compared to the modeled results from ADCIRC at 82 selected

locations in southeast Louisiana. These marks were selected because they were indicated as being still-water measurements of excellent quality, and thus the effects of wave action should be minimized. In addition, they are located east of Gustav's track and judged to not contain contributions from Ike, by comparing to hydrographs from the sources listed above.

4. Synoptic History and Validation of Gustav

The following sections describe the evolution of Gustav's winds (Figure 8), waves (Figure 9-10), and water levels (Figure 11) in southeast Louisiana and the validation of the wave and surge models using data at reliable stations. Although station time series of wave parameters are shown from WAM, STWAVE and SWAN, the water levels shown are produced via the coupling of SWAN+ADCIRC. Geographical locations referenced in the text are summarized in Table 1 and shown in Figure 1.

a. Evolution of Winds

Gustav tracked through the Caribbean Sea (Figure 4) and strengthened to a Category 4 storm on the Saffir-Simpson scale, with maximum 10min-averaged wind speeds of 69 m s^{-1} (Beven and Kimberlain, 2009). After passing over western Cuba and into the Gulf, Gustav weakened to Category 3 and maintained this intensity until dropping to Category 2 approximately 10hr before landfall. It progressed northwestward and made landfall as a Category 2 storm in Terrebonne Bay in southern Louisiana. This behavior is in contrast to Katrina and Rita, which reached their peak intensities as Category 5 storms while in the Gulf.

However, Gustav's outer extent of tropical-storm-strength winds was large enough to produce integrated kinetic energy values over 40 TJ, resulting in a rating of 3.0 (out of a possible 6.0) on the Surge Destructive Potential Scale at landfall (Powell and Reinhold, 2007). Tropical-

storm-strength winds reached the bird's foot of the Mississippi River delta approximately 12hr before landfall (Figure 8a) and enveloped large portions of southern Louisiana and the LA-MS continental shelf by 6hr before landfall (Figure 8b). Predominantly easterly coastal winds were relatively constant strength for 12-15hr as the storm moved through the region. On the shallow shelf, winds created local waves and surge, which were then pushed across the sounds and against the levee protection system. These winds also pushed surge into Lake Pontchartrain.

As Gustav neared landfall, its strongest winds were $30\text{-}35\text{ m s}^{-1}$, and they were limited to the narrow shelf to the southwest of the Mississippi River (Figure 8c-d). Barataria and Terrebonne Bays experienced the worst of the hurricane winds as it made landfall. However, by this late stage, the winds shifted quickly to onshore, and then continued onshore for several hours after landfall (Figure 8e), aligning with the lake/marsh system connecting northward from Barataria Bay to the west bank of New Orleans.

Winds continued southeasterly over the Louisiana-Mississippi shelf for more than 12hr after landfall (Figure 8f). Although the winds had weakened further, their direction over the shelf caused the winds to slow the recession of surge back into the deeper Gulf. The wind held the surge in Lake Pontchartrain, and it assisted the surge propagation over the Caernarvon Marsh to the east of the river and over the marshes to the south and west of New Orleans.

b. Evolution of Waves

Gustav generated waves with estimated significant heights of 12-15m in deep water in the northeast quadrant of the storm, where the winds were strongest. These waves propagated as swell in all directions, but were largest to the east of the track. NDBC buoys 42036, 42039 and 42040 are located in the northeastern Gulf between Tampa Bay and the Mississippi River delta (Figure 12), and their measured significant heights increased as the storm passed. At buoy

42040, the largest measured significant wave heights exceeded 10m (Figure 13). To the west of the track, wave heights decreased with distance from the track, with peak measured waves of 6m at NDBC buoy 42001 decreasing to 3m at buoys 42019 and 42020 nearer to Texas. As the storm passed, the mean wave periods also increased (Figure 14), and the mean wave directions changed dramatically (Figure 15).

In all of these validation plots, note the good agreement between the measured data and the computed results of WAM and SWAN. This agreement can be quantified through the use of the Scatter Index (SI):

$$SI = \frac{\sqrt{\frac{1}{N} \sum_{i=1}^N (E_i - \bar{E})^2}}{\frac{1}{N} \sum_{i=1}^N |O_i|},$$

and the normalized bias:

$$\text{Bias} = \frac{\frac{1}{N} \sum_{i=1}^N E_i}{\frac{1}{N} \sum_{i=1}^N |O_i|},$$

where N is the number of observations, $E_i = S_i - O_i$ is the error between the modeled (S_i) and measured (O_i) values, and \bar{E} is the mean error (Hanson *et al.*, 2009). Thus the SI is the ratio of the standard deviation of the measured-to-modeled errors to the mean measured value. Table 5 summarizes the mean SI and mean normalized bias errors for all of the wave data sets, where the mean is computed as an average over the individual stations. At the NDBC buoys, the mean SI errors for the significant wave heights for WAM and STWAVE are in the range of 0.26 to 0.28 and the mean normalized biases are -0.07 to 0.09, whereas the mean SI errors for SWAN are 0.31 to 0.32 and the mean normalized biases are 0.14 to 0.15. The slightly larger SI errors for SWAN are due to two of the NDBC buoys on the Louisiana-Texas continental shelf (42019 and

42020); as shown in Figure 13, the swell computed by SWAN at those buoys is too large. These buoys are farthest from Gustav's track in the Gulf and are located at the edge of the shelf break. We note that for other storms such as Katrina (2005), Rita (2005) and Ike (2008) with locally stronger and longer duration swell, these stations generally perform better with SWAN on the SL16 grid than for Gustav. Table 5 also includes the mean *SI* for the SWAN results at a sub-set of locations that are consistent with WAM/STWAVE, and a smaller sub-set without the NDBC buoys 42019 and 42020. When these buoys are removed from the analysis, the mean *SI* error for the significant wave heights for SWAN is 0.26, which is comparable to the errors produced by WAM and STWAVE. The mean *SI* errors for the peak and mean wave periods are similar for the three wave models.

The waves generated near the track in deep water also propagated northward, where they moved onto the LA-MS continental shelf and dissipated due to changes in bathymetry and bottom friction. The largest and longest waves reached the Mississippi River delta 3-6hr before landfall (as computed in Figure 9b-c and Figure 10b-c). These waves had significant heights of 10-12m and mean periods of 12-15s, and they dissipated quickly due to the steep, narrow shelf near the delta. As the storm approached landfall, its local hurricane-strength winds created large waves offshore of the Barataria and Terrebonne Bays (as computed in Figure 9c-d and Figure 10c-d). At CSI stations 6, 9 and 15 located in 18-20m of water depth (Figure 16), the measured significant heights at the peak of the storm were 7m (Figure 17), and the peak periods were 12-15s (Figure 18). The waves began to dissipate due to depth-limited breaking before reaching these stations and gages closer to shore. At CSI station 5 and at the AK gages 1, 8 and 9 located outside of Terrebonne Bay in 7-10m of water depth, the peak wave heights decreased to 3-5m. At AK gage 11 farther east near Barataria Bay and in 3.5m of water depth, the peak significant

heights were 1-2m, and the peak periods were 16s. As shown in Table 5, the mean *SI* errors for the CSI and AK data sets are similar for STWAVE and SWAN. The mean *SI* errors for the significant wave heights range from 0.31 to 0.42, while the mean *SI* errors for the wave periods range from 0.35 to 0.46. The mean normalized biases for the significant wave heights range from 0.20 to 0.38, while the mean normalized biases for the wave periods range from -0.07 to 0.27. Dissipation of the swell and local wind-sea waves is captured by the measured time series and matched well by STWAVE and SWAN.

To the east of the Mississippi River, tropical-storm-strength winds pushed waves onto the LA-MS continental shelf (as computed in Figure 9b-e and Figure 10b-e). At NDBC buoy 42007 and AK gage 12 located outside the Chandeleur Islands, peak waves were 6m, and they decreased farther east near Mobile and Pensacola Bays to 4m at AK gages 18, 19 and 20 (Figure 16-17). Wave heights decreased behind the barrier islands, such as at AK gage 17, which is located in 4.5m of water depth and had a peak wave height of 2m.

Shoreward of the barrier islands, which attenuated the larger waves propagating onshore from open water, predominantly local waves were generated within the sounds and marshes. They generally had mean periods less than 3s (as computed in Figure 10), and their significant heights were 2m in the sounds and lakes and 1m or less in the wetlands (as computed in Figure 9). Near landfall, CHL gages 10512, 10508 and 10514 measured local wave generation and dissipation within the marshes north of Terrebonne Bay; note the decrease in the wave heights from 0.8m to 0.5m at the northernmost gages. To the east of the river, the AK gages 13 and 14 measured 0.5-1m waves over the Caernarvon Marsh (Figure 17), while the CHL gages 10510, 10513 and 10504 measured 0.5-1m waves over the Biloxi Marsh (Figure 19). The peak periods were also small in the marshes, ranging from 2-4s at landfall (Figure 20), although the peak

periods may be underestimated due to the high-frequency cut-off of the gages, as described above. These measurements are excellent validation tests for STWAVE and SWAN, because they are located in regions with rapidly-changing bathymetry and bottom friction. As shown in Table 5, the mean *SI* and mean normalized bias errors are much larger at the CHL gages, for both the SWAN and STWAVE wave models. These larger values reflect the sensitivity of the error measure to the relatively smaller wave heights and periods measured by these gages, but they also reflect the sensitivity to bathymetric and local geometric details, the calculated surge, as well as the difficulty in parameterizing the bottom friction in these marshes. The measurements collected by these gages are invaluable in their description of the nearshore wave environment, and they provide an opportunity for improvement of the modeled physics.

c. Evolution of Storm Surge

As Gustav moved through the Gulf, its easterly and southeasterly winds blew with tropical-storm strength for 12-15hr over the LA-MS shelf. These winds also stretched to the Florida shelf, and they helped to create a surge of 0.5-1m at NOAA stations 8726724 and 8729108 (Figure 12 and 21). Although the storm was relatively weak in intensity as it traversed the Gulf, especially compared to other Gulf storms such as Katrina and Rita, its large size caused it to impact the coastline from the Florida Keys to Texas.

During this early part of the storm, the levees of lower Plaquemines Parish experienced more than 2m of surge (as computed in Figure 11b-c). Northeasterly winds pushed water across Breton Sound and against the river levees, which are relatively unprotected by marshes in their southernmost reach. AK gage 13 and CHL gage 10510 are located in the wetlands near the edge of Breton Sound (Figure 16), and they measured peak surge of 3-3.25m (Figure 22-23). The levee on the west bank in lower Plaquemines Parish extends farther south, and thus surge can

enter the Mississippi River from the east and then propagate up the deep and efficient river, as shown in the gages of the USACE (Figure 24). At gages south of the levees and near the delta, such as USACE gages 1545 and 1516, the surge was relatively small, with peaks of 1.5-2m (Figure 25). However, the surge was larger at the gages upriver. At USACE gages 1380 and 1300 in New Orleans, the peak surge was 2.5m above the pre-storm levels and 3m relative to NAVD88 (2004.65). At USACE gage 1220 near Donaldsonville, the surge attenuated to 2m above the pre-storm levels. The ADCIRC model applied a constant flow rate river radiation boundary condition to the Mississippi River using an average flow value during the storm equal to $8,920\text{m}^3\text{s}^{-1}$. It is clear from the river hydrographs (USACE gages 01220, 01260, 01275, 01300, 01380, 01545 shown in Figure 27) that the river is falling during this period and that a variable flow rate river radiation boundary condition should be used to improve model skill. It is noted that the storm period average flow rate is slightly above average for peak hurricane season. This surge did not overtop the levees along the river. However, surge would propagate similarly at higher flow rates with correspondingly higher pre-storm river stages, which are possible during hurricane season.

New Orleans was also threatened by surge in the channels in and around the city. Water in Mississippi Sound and Lake Borgne was pushed by northeasterly winds into the wetlands and the confluence of the MRGO and GIWW, and eventually into the IHNC. Water levels were 2.5-3m in Lake Borgne and higher in the canals (as computed in Figure 11c-d). This relatively fast process corresponded to water being blown efficiently through Lake Borgne and to the timing of the peak winds as Gustav made landfall. At NOAA 8761305 (Figure 21), USACE 76010 (Figure 25), and the deployable USGS STB-04 (Figure 27), which are located along the MRGO and the south shore of Lake Borgne, note the sharp peak of 3.25m in the water levels at 1400

UTC 01 September 2008. This surge was focused by the confluence and reached higher levels of 3.5-3.75m within the IHNC. This trend is shown at gages located at the entrance to the IHNC (deployable USGS ORL-13) and within the southern reach of the IHNC (USACE 76160 and deployable USGS ORL-08). The peaks are narrow in these hydrographs, indicating that the surge enters and recedes quickly in the canal-lake-sound system. This 3.5-3.75m of surge in the IHNC was a serious threat to New Orleans. The levees were not breached, however, water levels were within 0.5m of the tops of the levees, and some wave overtopping was reported.

As computed in Figure 11b-f, the Biloxi and Caernarvon marshes tend to slow the time of arrival of the surge but do not significantly attenuate the peaks due to the sustained northeasterly-to-southeasterly winds. The CHL gages 10510, 10513 and 10504 show the limited dissipation of the surge as it moved over and around (through the Mississippi Sound and Lake Borgne) the friction-dominated Biloxi marsh. Note the decrease of 0.25m in the peak surge at these gages from east to west (Figure 23). The Caernarvon marsh also caused limited dissipation of the peak surge. At AK gage 13 located at the edge of the marsh, the peak surge is 3.35m, whereas the surge is 2.25m at AK gage 14 in Lake Lery (Figure 22). Farther north against the levees, the permanent USGS gage 295124089542100 also shows a peak of 2.25m. This surge existed against the levees of lower Plaquemines Parish, prior to being pushed northward over the marsh by the shifting winds. The marshes are believed to attenuate surge by as much as 1m per 14.5km (USACE, 1963; Resio and Westerink, 2008). However, after the winds shifted, the surge pushed effectively over the marshes; note the lack of attenuation in the Caernarvon marsh 9-12hr after landfall (as computed in Figure 11f). Similar to other hurricanes that have impacted the region, when Gustav's winds aligned northwestward for an extended period over the marshes, surge was pushed effectively against the levees in the vicinity of English Turn.

From the north, the city experienced surge along the levees at the south shore of Lake Pontchartrain. Before landfall, northeasterly winds pushed surge within the lake; note the northeast-to-southwest gradient in the lake in Figure 11b-c. However, as the storm made landfall and the winds shifted, surge was pushed around the barrier islands, through Lake Borgne and the passes, and into Lake Pontchartrain. Note the surges of 2.25m at AK gage 17 (Figure 22) and 3.25m at the NOAA station 8747437 (Figure 21) located near the entrance to Lake Borgne. This flow into the lake was caused by the easterly and southeasterly winds and by a strong gradient between the lakes (as computed in Figure 11c-e). This exchange is shown at the permanent USGS gages 301001089442600 and 30830089515000 in eastern Lake Pontchartrain (Figure 26); the lake fills over the second half of 01 September 2008 and then drains gradually over 02-03 September 2008 (Figure 27). As measured at NOAA station 8761927 (Figure 21), the USACE gages 85575, 85625 and 85670 (Figure 24-26), and the deployable USGS gages ORL-02, ORL-10 and ORL-14 (Figure 27), the maximum surge levels in the lake were 1.5-2m, but they occurred 9-12hr after landfall, when the lake had come to an equilibrium with Lake Borgne (as computed in Figure 11f). This behavior is matched well by ADCIRC at all gages.

Finally, on the west bank of the river, the surge was smaller, but it propagated far inland and approached the west bank of New Orleans. As Gustav made landfall, its winds shifted southerly over Barataria Bay, creating surge of 1.5-2.25m along Grand Isle and adjacent barrier islands (as computed in Figure 11d). As measured at NOAA stations 8761724 and 8762075 and AK gage 11, the coastal surge built and receded quickly. However, much of the surge pushed inland because the winds continued to blow southerly for more than 12hr after landfall. Surge propagated into the marsh/lake system through Little Lake, Lake Salvador and Lake Cataouatche, located south of New Orleans. As the surge moved northward, it became less

peaked in the hydrographs. At the permanent USGS gages 292800090060000 and 07380335 located in Little Lake, the peak surge is 1.5m and occurs 6-8hr after landfall (Figure 27). Farther north, at the USACE gages 82875, 76230 and 76240 and USGS permanent gage 2951190901217 located near Lake Salvador, the peak surge is 1m and persists for 12-36hr after landfall (Figure 25). Farther west, at the CHL gages 10512, 10508 and 10514 located in the marsh north of Terrebonne Bay, the inland push and slow recession is also evident in the days following landfall (Figure 23). There appears to be too much attenuation in the surge signals at CHL gages 10508 and 10514, indicating locally insufficient resolution of fine scale channels that provide conveyances that are important in getting the relatively quick surge into the system. Thus frictional resistance and conveyance resolution are especially important when the time scale of the flow is fast.

Overall, ADCIRC correlates well to water levels throughout the region, including at most of the hydrographs herein. The mean *SI* errors for the time series of water levels are summarized in Table 6. The mean *SI* errors for the offshore (CSI and AK) and open-water (NOAA) stations and gages range from 0.27 to 0.37, while the mean normalized biases range from -0.04 to 0.20. The rest of the measured time series are inland, and the mean errors are smaller at these locations, with *SI* ranging from 0.19 to 0.27 and normalized biases ranging from 0.04 to 0.20. The level of skill of ADCIRC reflects the relative uncertainties of the bathymetry and bottom friction, the errors in vertical datums, as well as the mesh resolution used to define features. Further refinement of the mesh throughout the region, especially in connection with the ever-improving input data for bathymetry, topography and land use, would continue to improve the model results. However, the overall mean *SI* error of 0.24 and mean normalized bias of 0.14 for the ADCIRC water levels indicates a high level of performance during this Gustav hindcast.

This behavior is confirmed by a comparison to measured HWMs from FEMA and peak values from all 365 hydrographs included in the analysis in Table 6. In Figure 28, the points are color-coded based on the error (modeled less measured); warm colors indicate locations where ADCIRC over-predicted the peak water level, while cool colors indicate locations where ADCIRC under-predicted the peak water level. The modeled peak water levels are within 0.5m at 375 of the 408 (92 percent) measured peaks that were wetted by ADCIRC. In a scatter plot of measured-to-modeled peaks, the CRMS data have a best-fit slope of 0.97 and an R^2 of 0.70, while the FEMA data have a best-fit slope of 0.94 and an R^2 of 0.82. When all of the data sets are combined, the best-fit line has a slope of 0.95 and R^2 of 0.81, as shown in Figure 29. Some portion of these differences can be attributed to measurement error, which is quantified using an estimation method described by Bunya *et al.* (2010). When the measurement error is taken into account (Table 6), the average absolute ADCIRC error is 0.14m, and the standard deviation is 0.22m.

This level of model skill can be attributed to the mesh resolution of the SL16 mesh and the representation of detailed features, but it is also a result of the wave-current interaction and the resulting wave-induced set-up. Figure 30 shows the wave-induced water level set-up resulting from coupling STWAVE+ADCIRC and SWAN+ADCIRC. The STWAVE and SWAN models generally lead to very similar wave-induced set-up as large as 0.5m for Gustav. Behind the breaking zones, the wave-induced set-up from both models accounts for 0.1-0.3m throughout much of the region, and 0.5m in regions near the high-gradient shallow-water wave dissipation zones. These contributions can be locally significant when compared to the overall peak water levels, which were 2-3m in the marshes and lakes behind the barrier islands. Differences between the STWAVE and SWAN model couplings to ADCIRC are attributable to

the wave model domain extent, grid resolution, and most importantly to the way in which waves are dissipated. Wave dissipation in STWAVE is more localized leading to a more rapid spatial gradient in wave heights and higher peak wave radiation stress gradients in shallower depths. The peaks in its set-up are therefore larger in the vicinity of the Chandeleur Islands and the Mississippi River delta. SWAN spreads its dissipation over a larger area.

5. Conclusions

Gustav made landfall as a Category 2 storm at Cocodrie, LA, and near Terrebonne Bay in southern Louisiana. Its strongest winds were concentrated west of the Mississippi River, and its largest waves dissipated along the delta and continental shelf break. However, because of its large size, the hurricane blew strong winds over the LA-MS shelf, pushing surge through the Mississippi Sound and Lake Borgne, over the marshes and against the levee system of metropolitan New Orleans. The highest water levels were observed in the channels near the city, and levees were threatened with overtopping and breaching. New Orleans was protected by its levees, the marshes to the south and east, the relative weakness of the storm, and the distance from landfall. Nevertheless, Gustav created significant surge on all sides of the city.

An unprecedented amount of wave and water level data were collected for Hurricane Gustav, and, together with high-quality data-assimilated winds, they allow for a thorough assessment of the performance of the WAM, STWAVE, SWAN, and ADCIRC models in simulating the physics of hurricane waves and surge from the deep Gulf of Mexico to the inland portions of the coastal floodplain. It is especially important that most of this data is in the form of time histories, which allow for an evaluation of the durations and timing of processes, and thus an understanding of the frictional dynamics of process propagation, attenuation, and/or recession.

As Gustav moved in deep water, it created large waves that radiated outward and impacted most of the Gulf. The waves had estimated significant heights of 15m nearer to the storm's track. NDBC buoys measured waves with significant heights of 8-10m, and the timing and magnitudes of these waves are matched well by WAM and SWAN. In shallow water, the nearshore instruments of CSI platforms and AK buoys measured the waves as they were dissipated on the continental shelf. Waves were further dissipated by the barrier islands, and predominantly local waves were generated and dissipated in the marshes, as shown by the gages of AK and CHL. Overall, as shown in Table 5, the three wave models perform similarly with respect to their mean *SI* and mean normalized bias errors. In the Gulf of Mexico deep and shelf waters, WAM overall performed slightly better for significant wave heights while SWAN produces a smaller mean *SI* and mean normalized bias for peak and mean wave periods. For this storm, WAM simulates better significant wave heights for the short duration lower energy swell for the NDBC buoys at the edge of the Texas shelf. Inner-shelf, open-water wave characteristics are similarly and generally well modeled by STWAVE and SWAN. Further work is necessary to determine propagation and dissipation characteristics for swell onto and across shelves, as well as across rapid topographic transitions such as barrier islands by looking at a range of storms and by collecting additional wave data in the vicinity of these features. This will improve our understanding of wave transformation as well as wave radiation stress gradients in shallow water, which in turn drive coastal wave-induced set-up and currents. Improved accuracy of bathymetry/topography and the associated mesh resolution will also help improve wave modeling skill, particularly in shallow waters where depth-limited breaking dominates. Presently, many parts of coastal Louisiana are still very poorly surveyed, with many bathymetric values dating back more than 50 years. At the marsh locations measured by the CHL gages, the

mean *SI* and mean normalized bias errors are large for both STWAVE and SWAN, indicating that both models require further work to improve their bottom friction and dissipation through porous wetlands systems.

Gustav's large size caused its tropical-storm-strength winds to impact the region for 12-15hr before and during landfall, and these winds pushed surge across the LA-MS shelf and against the levees of lower Plaquemines Parish. Surge of 2-2.75m above the pre-storm levels was pushed up the Mississippi River, and surge of 3-3.5m was pushed into the IHNC. The peak surge occurred east of the river, in regions where the maximum winds did not reach, because the storm was large enough in size to blow medium-strength winds over the shelf for an extended length of time. In Lake Pontchartrain, water levels increased to 1.5-2m as surge was pushed through the Rigolets and Chef Menteur passes. To the southwest, the Caernarvon and Biloxi marshes are widely believed to attenuate storm surge by as much as 3m, but the surge from the levees along lower Plaquemines Parish was pushed northward effectively over the marshes and against the levees near Braithwaite and English Turn. The marshes offered little protection as the water levels were within 0.5m of the tops of the levees. Finally, the interconnected marshes south and west of New Orleans allowed storm surge to propagate from the landfall location and threaten the city many hours after the storm passed. Surge of 0.75-1m was observed on the west bank even 12-36hr after landfall.

The storm surge is also described by a wealth of measured water level data, and ADCIRC correlates well with its water levels. The overall mean *SI* error was 0.24 and mean normalized bias was 0.14 at 362 measurement locations, and the modeled peak water levels were within 0.5m at 92 percent of the HWMs and peak hydrograph values. The timing of peaks, rise rates, and recession rates were captured well by ADCIRC. This level of model skill results from the

increased resolution of the SL16 mesh which represents small-scale channels and conveyances as well as the use of spatially varying Manning's n based friction. Improvements in modeling inland surge can be achieved by developing a time dependent river radiation boundary condition to allow for time varying river inflows; further refining flow conveyances penetrating into the floodplain; and by perfecting the representation of wetland friction to consider the complex fine scale channels as well as the change in character that occurs during a storm including considering the transition from emergent to submerged and the flattening of wetland grasses as the storm progresses.

Acknowledgments

This work was supported by the U.S. Army Corps of Engineers (USACE) New Orleans District and the Federal Emergency Management Agency Region 6. Computational resources and support were provided by the U.S. Army Engineer Research and Development Center, Department of Defense Supercomputing Resource Center and the University of Texas at Austin, Texas Advanced Computing Center. Awards from the National Science Foundation (OCI-0746232) and the Office of Naval Research (N00014-06-1-0285) supported ADCIRC and SWAN model development. Permission to publish this paper was granted by the Chief of Engineers, U.S. Army Corps of Engineers.

References

Amante, C., and B. W. Eakins, 2009: ETOPO1 1 Arc-Minute Global Relief Model: Procedures, Data Sources and Analysis. *NOAA Technical Memorandum NESDIS NGDC-24*, 19 pp.

Battjes J.A., and J.P.F.M. Janssen, 1978: Energy loss and set-up due to breaking of random waves. *Proc. 16th Int. Conf. Coastal Engng.*, ASCE, 1978, 569–587.

Beven, J.L., and T.B. Kimberlain, 2009: Tropical Cyclone Report, Hurricane Gustav, 25 August - 4 September 2009. NOAA/National Hurricane Center, 38 pp.

Booij, N., R.C. Ris, and L.H. Holthuijsen, 1999: A third-generation wave model for coastal regions, Part I, Model description and validation. *J. Geoph. Research* 104, 7649-7666.

Bretschneider, C.L., H.J. Krock, E. Nakazaki, and F.M. Casciano, 1986: Roughness of Typical Hawaiian Terrain for Tsunami Run-Up Calculations: A Users Manual. J.K.K. Look Laboratory Report, University of Hawaii, Honolulu.

Buczowski, B.J., Reid, J.A., Jenkins, C.J., Reid, J.M., Williams, S.J., and Flocks, J.G., 2006: usSEABED: Gulf of Mexico and Caribbean (Puerto Rico and U.S. Virgin Islands) offshore surficial sediment data release. *U.S. Geological Survey Data Series 146, version 1.0*. Online at <http://pubs.usgs.gov/ds/2006/146/>

Bunya, S., J.C. Dietrich, J.J. Westerink, B.A. Ebersole, J.M. Smith, J.H. Atkinson, R. Jensen, D.T. Resio, R.A. Luettich, C. Dawson, V.J. Cardone, A.T. Cox, M.D. Powell, H.J. Westerink, H.J. Roberts, 2010: A High-Resolution Coupled Riverine Flow, Tide, Wind, Wind Wave and Storm Surge Model for Southern Louisiana and Mississippi: Part I - Model Development and Validation. *Monthly Weather Review*, 138(2), 345-377.

Cardone, V.J., 1969: Specification of the wind distribution in the marine boundary layer for wave forecasting. Tech Rep 69-1, Geophys Sci Lab, NYU.

Cardone, V.J., and A.T. Cox, 2007: Tropical cyclone wind field forcing for surge models: Critical issues and sensitivities. *Nat. Hazards*, 51, 29-47.

Cox, A.T., J.A. Greenwood, V.J. Cardone, and V.R. Swail, 1995: An interactive objective kinematic analysis system. *Proc. Fourth Int. Workshop on Wave Hindcasting and Forecasting*, Banff, Alberta, Canada, Atmospheric Environment Service, 109-118.

Dawson, C., J.J. Westerink, J.C. Feyen, and D. Pothina, 2006: Continuous, Discontinuous and Coupled Discontinuous-Continuous Galerkin Finite Element Methods for the Shallow Water Equations. *Int. J. Numer. Meth. Fluids*, 52, 63-88.

Dietrich, J.C, S. Bunya, J.J. Westerink, B.A. Ebersole, J.M. Smith, J.H. Atkinson, R. Jensen, D.T. Resio, R.A. Luettich, C. Dawson, V.J. Cardone, A.T. Cox, M.D. Powell, H.J. Westerink, H.J. Roberts, 2010: A High-Resolution Coupled Riverine Flow, Tide, Wind, Wind Wave and

Storm Surge Model for Southern Louisiana and Mississippi: Part II - Synoptic Description and Analysis of Hurricanes Katrina and Rita. *Monthly Weather Review*, 138(2), 378-404.

Dietrich, J.C., M. Zijlema, J.J. Westerink, L.H. Holthuijsen, C. Dawson, R.A. Luetlich, R. Jensen, J.M. Smith, G.S. Stelling, and G.W. Stone, 2011: Modeling Hurricane Waves and Storm Surge using Integrally-Coupled, Scalable Computations. *Coastal Engineering*, 58, 45-65, DOI: 10.1016/j.coastaleng.2010.08.001.

Ebersole, B.A., J.J. Westerink, D.T. Resio, and R.G. Dean, 2007: Performance evaluation of the New Orleans and Southeast Louisiana Hurricane Protection System, Volume IV - The storm. Final Report of the Interagency Performance Evaluation Task Force, U.S. Army Corps of Engineers, Washington, DC, 263 pp.

FEMA, 2009a: Flood Insurance Study: Southeastern Parishes, Louisiana, Intermediate Submission 2: Offshore Water Levels and Waves, US Army Corps of Engineers, New Orleans District.

FEMA, 2009b: Louisiana Hurricane Ike Coastal High Water Mark Data Collection, FEMA-1792-DR-Louisiana, Draft Report, February 2009.

Garster, J. K., B. Bergen, and D. Zilkoski, 2007: Performance evaluation of the New Orleans and Southeast Louisiana Hurricane Protection System, Volume II—Geodetic vertical and water level

datums. Final Report of the Interagency Performance Evaluation Task Force, U.S. Army Corps of Engineers, Washington, DC, 157 pp.

Günther, H., 2005: WAM cycle 4.5 version 2.0. Institute for Coastal Research, GKSS Research Centre, Geesthacht, Germany, 38 pp.

Hanson, J.L., B.A. Tracy, H.L. Tolman, and R.D. Scott, 2009: Pacific hindcast performance of three numerical wave models. *J. Atmospheric and Oceanic Technology*, 26, 1614-1633.

Hasselmann S., K. Hasselmann, J.H. Allender, and T.P. Barnett, 1985: Computations and parameterizations of the nonlinear energy transfer in a gravity wave spectrum. Part II: parameterizations of the nonlinear transfer for application in wave models. *J. Phys. Oceanogr.*, 15(11), 1378-1391.

Holland, G., 1980: An analytic model of the wind and pressure profiles in hurricanes. *Monthly Weather Review*, 108, 1212–1218.

Janssen, P.A.E.M., 1991: Quasi-linear theory of wind-wave generation applied to wave forecasting. *Journal of Physical Oceanography*, 21, 1631-1642.

Kennedy, A.B., U. Gravois, B. Zachry, R.A. Luettich, T. Whipple, R. Weaver, J. Fleming, Q.J. Chen, and R. Avissar, 2010: Rapidly Installed Temporary Gauging for Waves and Surge during Hurricane Gustav. *Continental Shelf Research*, 30, 1743-1752.

Kennedy, A.B., U. Gravois, B. Zachry, J.J. Westerink, M. Hope, J.C. Dietrich, M.D. Powell, A.T. Cox, R.L. Luettich, and R.G. Dean, 2011: Origin of the Hurricane Ike Forerunner Surge. *Geophysical Research Letters*, in review.

Knabb, R.D., J.R. Rhome, and D.P. Brown, 2005: Tropical cyclone report, Hurricane Katrina, 23-30 August 2005. NOAA/National Hurricane Center, 43 pp.

Kolar, R.L., J.J. Westerink, M.E. Cantekin, and C.A. Blain, 1994: Aspects of nonlinear simulations using shallow water models based on the wave continuity equations. *Computers and Fluids*, 23(3), 1-24.

Komen, G., L. Cavaleri, M. Donelan, K. Hasselmann, S. Hasselmann, and P.A.E.M. Janssen, 1994: *Dynamics and Modeling of Ocean Waves*. Cambridge University Press, 560 pp.

Luettich, R.A., and J.J. Westerink, 2004: Formulation and Numerical Implementation of the 2D/3D ADCIRC Finite Element Model Version 44.XX; 2004. http://adcirc.org/adcirc_theory_2004_12_08.pdf

Madsen, O.S., Y.-K. Poon and H.C. Graber, 1988: Spectral wave attenuation by bottom friction: Theory, *Proc. 21th Int. Conf. Coastal Engineering*, ASCE, 492-504.

NOAA National Geophysical Data Center, NGDC Coastal Relief Model, Retrieved 01 December 2008, <http://www.ngdc.noaa.gov/mgg/coastal/coastal.html>

Powell, M., S. Houston, and T. Reinhold, 1996: Hurricane Andrew's landfall in South Florida. Part I: Standardizing measurements for documentation of surface wind fields. *Wea. Forecasting*, 11, 304-328.

Powell, M. S. Houston, L. Amat, and N. Morrisseau-Leroy, 1998: The HRD real-time hurricane wind analysis system. *J. Wind Eng. Ind. Aerodyn.*, 77-78, 53-64.

Powell, M.D., P.J. Vickery, and T.A. Reinhold, 2003: Reduced drag coefficient for high wind speeds in tropical cyclones. *Nature*, 422, March 20, 279-283.

Powell, M., 2006: Drag Coefficient Distribution and Wind Speed Dependence in Tropical Cyclones. *Final Report to the National Oceanic and Atmospheric Administration (NOAA) Joint Hurricane Testbed (JHT) Program.*

Powell, M. D. and T. A. Reinhold, 2007: Tropical cyclone destructive potential by integrated kinetic energy. *Bull. Amer. Meteor. Soc.*, 88, 513-526.

Powell, M. D., S. Murillo, P. Dodge, E. Uhlhorn, J. Gamache, V. Cardone, A. Cox, S. Otero, N. Carrasco, B. Annane, and R. St. Fleur, 2010: Reconstruction of Hurricane Katrina's wind fields for storm surge and wave hindcasting. *Ocean Engineering*, 37, 26-36.

Resio, D.T. and J.J. Westerink, 2008: Hurricanes and the Physics of Surges. *Physics Today*, 61, 9, 33-38.

Ris, R.C., N. Booij, and L.H. Holthuijsen, 1999: A third-generation wave model for coastal regions, Part II, Verification. *J. Geoph. Research*, 104, 7667-7681.

Rogers, W.E., P.A. Hwang, and D.W. Wang, 2003: Investigation of wave growth and decay in the SWAN model: three regional-scale applications. *J. Phys. Oceanogr.*, 33, 366-389.

Sheremet, A., and G.W. Stone, 2003: Observations of nearshore wave dissipation over muddy sea beds. *J. Geoph. Research*, 108, 3357-3368.

SiadatMousavi, S.M., F. Jose, and G.W. Stone, 2009: Simulating Hurricane Gustav and Ike Wave Fields along the Louisiana Innershelf: Implementation of an Unstructured Third-Generation Wave Model, SWAN. *Proceedings of the Oceans 2009 Conference*, Biloxi, MS, 873-880.

Smith, J.M., 2000: Benchmark tests of STWAVE. *Proc. Sixth Int. Workshop on Wave Hindcasting and Forecasting*, Monterey, CA, Environment Canada, 369-379.

Smith, J.M., A.R. Sherlock, and D.T. Resio, 2001: STWAVE: Steady-state spectral wave model user's manual for STWAVE, version 3.0. USACE, Engineer Research and Development Center, Tech. Rep. ERDC/CHL SR-01-1, Vicksburg, MS, 81 pp.

Smith, J.M., 2007. Full-plane STWAVE: II. Model overview. ERDC TN-SWWRP-07-5. Vicksburg, MS: U.S. Army Engineer Research and Development Center. <https://swwrp.usace.army.mil/>

Smith, J.M., R.E. Jensen, A.B. Kennedy, J.C. Dietrich, and J.J. Westerink, 2011: Waves in Wetlands: Hurricane Gustav. *Proceedings of the 32nd International Conference on Coastal Engineering*, in review.

Snyder R.L., F.W. Dobson, J.A. Elliott, and R.B. Long, 1981: Array measurements of atmospheric pressure fluctuations above surface gravity waves. *J. Fluid Mech*, 102, 1–59.

Uhlhorn, E. W., P. G. Black, J. L. Franklin, M. Goodberlet, J. Carswell, and A. S. Goldstein, 2007: Hurricane surface wind measurements from an operational stepped frequency microwave radiometer. *Mon. Wea. Rev.*, 135, 3070-3085.

USACE, 1963: *Interim Survey Report, Morgan City, Louisiana and Vicinity*, serial no. 63, US Army Engineer District, New Orleans, LA.

USACE, 2009: Hydraulics and Hydrology Appendix, *Louisiana Coastal Protection and Restoration: Final Technical Report*, US Army Engineer District, New Orleans, LA, 389 pp.

Vickery, P. J., Wadhera, D., Powell, M. D., and Y. Chen, 2009: A hurricane boundary layer and wind field model for use in engineering applications. *J. Appl. Meteor. Climate*, 48, 381-405.

Walters, D.J., 2009: Personal communication.

Westerink, J.J., R.A. Luetich, J.C. Feyen, J.H. Atkinson, C. Dawson, H.J. Roberts, M.D. Powell, J.P. Dunion, E.J. Kubatko, and H. Pourtaheri, 2008: A Basin to Channel Scale Unstructured Grid Hurricane Storm Surge Model Applied to Southern Louisiana. *Monthly Weather Review*, 136(3), 833-864.

Zijlema M., 2010: Computation of wind-wave spectra in coastal waters with SWAN on unstructured grids. *Coastal Engineering*, 57, 267-277.

List of Figure Captions

Figure 1: Schematic of southeastern Louisiana. Solid lines indicate Gustav's track (black), ADCIRC levee/road boundaries (brown) and the coastline (gray). Geographic locations of interest are indicated by numbers identified in Table 1.

Figure 2: Photographs during Gustav of (a) waves overtopping the IHNC walls near the Ninth Ward, and (b) surge overtopping the earthen levee near Braithwaite, courtesy of Nancy Powell, USACE.

Figure 3: Schematics of the azimuthal wind drag, showing: extents of sectors in relation to direction of storm movement (left),

Figure 4: Bathymetry (m) of the SL16 mesh. Gustav's track is shown with a solid black line.

Figure 5: Bathymetry/topography (m) of the SL16 mesh in southeastern Louisiana.

Figure 6: Mesh resolution (m) of the SL16 mesh in southeastern Louisiana.

Figure 7: Manning's n values for the SL16 mesh in southeastern Louisiana.

Figure 8: Wind speeds (m s^{-1}) in southeastern Louisiana during Hurricane Gustav. The panels correspond to the following times: (a) 0200 UTC 01 September 2008 or approximately 12hr before landfall, (b) 0800 UTC 01 September 2008 or approximately 6hr before landfall, (c) 1100

UTC 01 September 2008 or approximately 3hr before landfall, (d) 1400 UTC 01 September 2008 or approximately landfall, (e) 1700 UTC 01 September 2008 or approximately 3hr after landfall, (f) 0200 UTC 02 September 2008 or approximately 12hr after landfall.

Figure 9: Contours of SWAN significant wave heights (m) and vectors of wind speeds (m s^{-1}) in southeastern Louisiana during Hurricane Gustav. The panels correspond to the following times: (a) 0200 UTC 01 September 2008 or approximately 12hr before landfall, (b) 0800 UTC 01 September 2008 or approximately 6hr before landfall, (c) 1100 UTC 01 September 2008 or approximately 3hr before landfall, (d) 1400 UTC 01 September 2008 or approximately landfall, (e) 1700 UTC 01 September 2008 or approximately 3hr after landfall, (f) 0200 UTC 02 September 2008 or approximately 12hr after landfall.

Figure 10: Contours of SWAN mean wave periods (s) and vectors of wind speeds (m s^{-1}) in southeastern Louisiana during Hurricane Gustav. The panels correspond to the following times: (a) 0200 UTC 01 September 2008 or approximately 12hr before landfall, (b) 0800 UTC 01 September 2008 or approximately 6hr before landfall, (c) 1100 UTC 01 September 2008 or approximately 3hr before landfall, (d) 1400 UTC 01 September 2008 or approximately landfall, (e) 1700 UTC 01 September 2008 or approximately 3hr after landfall, (f) 0200 UTC 02 September 2008 or approximately 12hr after landfall.

Figure 11: Contours of ADCIRC water levels (m relative to NAVD88 2004.65) and vectors of wind speeds (m s^{-1}) in southeastern Louisiana during Hurricane Gustav. The panels correspond to the following times: (a) 0200 UTC 01 September 2008 or approximately 12hr before landfall,

(b) 0800 UTC 01 September 2008 or approximately 6hr before landfall, (c) 1100 UTC 01 September 2008 or approximately 3hr before landfall, (d) 1400 UTC 01 September 2008 or approximately landfall, (e) 1700 UTC 01 September 2008 or approximately 3hr after landfall, (f) 0200 UTC 02 September 2008 or approximately 12hr after landfall.

Figure 12: Locations of wave NDBC buoys (green points) and NOAA water level stations (blue points) in the Gulf of Mexico. The Gustav track is shown in black, the coastline and water bodies are shown in gray, and the boundaries of the SL16 mesh are shown in brown. Unlabeled NOAA water level stations are included in the analysis in Table 6, but their time series plots are not shown in Figure 21.

Figure 13: Time series of significant wave heights (m) at the 12 NDBC buoys shown in Figure 12. Measured NDBC values are shown with gray circles, while modeled results from SWAN (green), WAM (red) and STWAVE (blue) are shown with solid lines. Buoy 42003 stopped recording as the storm passed.

Figure 14: Time series of mean periods (s) at the 12 NDBC buoys shown in Figure 12. Measured NDBC values are shown with gray circles, while modeled results from SWAN (green), WAM (red) and STWAVE (blue) are shown with solid lines. Buoy 42003 stopped recording as the storm passed.

Figure 15: Time series of mean directions ($^{\circ}$) at the 12 NDBC buoys shown in Figure 12. Measured NDBC values are shown with gray circles, while modeled results from SWAN

(green), WAM (red) and STWAVE (blue) are shown with solid lines. Buoy 42003 stopped recording as the storm passed.

Figure 16: Locations of the nearshore AK gages (green points), CHL gages (blue points) and CSI stations (red points) in the northern Gulf of Mexico. The Gustav track is shown in black, the coastline and water bodies are shown in gray, and the boundaries of the SL16 mesh are shown in brown.

Figure 17. Time series of significant wave heights (m) at the 16 AK gages and five CSI gages shown in Figure 16. Measured values are shown with gray circles, modeled results from SWAN (green) and STWAVE (blue) are shown with solid lines.

Figure 18: Time series of peak wave periods (s) at the 16 AK gages and five CSI gages shown in Figure 16. Measured values are shown with gray circles, modeled results from SWAN (green) and STWAVE (blue) are shown with solid lines.

Figure 19: Time series of significant wave heights (m) at the six CHL gages shown in Figure 16. Measured values are shown with gray circles, modeled results from SWAN (green) and STWAVE (blue) are shown with solid lines.

Figure 20: Time series of peak wave periods (s) at the six CHL gages shown in Figure 16. Measured values are shown with gray circles, modeled results from SWAN (green) and STWAVE (blue) are shown with solid lines.

Figure 21: Time series of water levels (m relative to NAVD88 2004.65) at the 12 selected NOAA stations labeled in Figure 12. Measured NOAA values are shown with gray circles, and modeled ADCIRC results are shown with a green line.

Figure 22: Time series of water levels (m relative to NAVD88 2004.65) at the 16 AK gages and five CSI gages shown in Figure 16. Measured values are shown with gray circles, and modeled ADCIRC results are shown with a green line.

Figure 23: Time series of water levels (m relative to NAVD88 2004.65) at the six CHL gages shown in Figure 16. Measured values are shown with gray circles, and modeled ADCIRC results are shown with a green line.

Figure 24: Locations of the USACE water level stations (blue points) in southeastern Louisiana. The Gustav track is shown in black, the coastline and water bodies are shown in gray, and the boundaries of the SL16 mesh are shown in brown. Unlabeled USACE stations are included in the analysis in Table 6, but their time series plots are not shown in Figure 25.

Figure 25: Time series of water levels (m relative to NAVD88 2004.65) at the 18 selected USACE stations labeled in Figure 24. Measured USACE values are shown with gray circles, while modeled ADCIRC results are shown with a green line.

Figure 26: Locations of the permanent USGS water level stations (blue points) and deployable USGS water level gages (green points) in southeastern Louisiana. The Gustav track is shown in black, the coastline and water bodies are shown in gray, and the boundaries of the SL16 mesh are shown in brown. Unlabeled USGS stations are included in the analysis in Table 6, but their time series plots are not shown in Figure 27.

Figure 27: Time series of water levels (m relative to NAVD88 2004.65) at the selected nine permanent USGS stations and six deployable USGS gages labeled in Figure 26. Measured USGS values are shown with gray circles, and modeled ADCIRC results are shown with a green line.

Figure 28: Locations of the 82 URS/FEMA HWMs (circles) and 362 hydrographs (squares) in southeastern Louisiana. The points are color-coded to show the errors (modeled less measured) between the peak water levels; green points indicate matches within 0.5m. Warm colors indicate locations where ADCIRC over-predicted the peak water level, while cool colors indicate locations where ADCIRC under-predicted the peak water level. White points indicate locations that were never wetted by ADCIRC.

Figure 29: Scatterplot of FEMA HWMs (circles) and peak hydrograph water levels (squares) for Gustav. Green points indicate a match within 0.5m. Red, orange, yellow and light green circles indicate overprediction by the model; green, blue, dark blue and purple circles indicate underpredictions. The slope of the best-fit line through all points is 0.95 and the R^2 value is 0.81.

Figure 30: Maximum Gustav event wave-induced set-up produced by coupling ADCIRC to (a) STWAVE and (b) SWAN. The extents of the two structured STWAVE domains are shown in blue lines.

Tables

Table 1: Geographic location by type and number shown in Figure 1.

Rivers and channels	
1	Rigolets
2	Chef Menteur Pass
3	Gulf Intracoastal Waterway (GIWW)
4	Mississippi River Gulf Outlet (MRGO)
5	Inner Harbor Navigational Canal (IHNC)
6	Mississippi River
Bays, lakes and sounds	
7	Chandeleur Sound
8	Breton Sound
9	Lake Borgne
10	Lake Pontchartrain
11	Lake Cataouatche
12	Lake Salvador
13	Little Lake
14	Barataria Bay
15	Terrebonne Bay
Islands	
16	Dauphin Island
17	Mississippi Sound Islands
18	Chandeleur Islands
19	Grand Isle
Places	
20	Louisiana-Mississippi Shelf
21	Biloxi Marsh
22	Caernarvon Marsh
23	"Bird's Foot" of the Mississippi River Delta
24	Plaquemines Parish
25	English Turn
26	Braithwaite
27	New Orleans
28	Port Fourchon

Table 2: Manning's n values for LA-GAP classification.

LA-GAP Class	Description	Manning's n
1	Fresh marsh	0.065
2	Intermediate marsh	0.055
3	Brackish marsh	0.050
4	Saline marsh	0.035
5	Wetland forest deciduous	0.140
6	Wetland forest evergreen	0.160
7	Wetland forest mixed	0.150
8	Upland forest deciduous	0.160
9	Upland forest evergreen	0.180
10	Upland forest mixed	0.170
11	Dense pine thicket	0.180
12	Wetland scrub/shrub deciduous	0.065
13	Wetland scrub/shrub evergreen	0.080
14	Wetland scrub/shrub mixed	0.070
15	Upland scrub/shrub deciduous	0.075
16	Upland scrub/shrub evergreen	0.090
17	Upland scrub/shrub mixed	0.080
18	Agriculture/crops/grass	0.050
19	Vegetated urban	0.120
20	Non-vegetated urban	0.120
21	Wetland barren	0.030
22	Upland barren	0.035
23	Water	0.025

Table 3: Manning's n values for MS-GAP classification.

MS-GAP Class	Description	Manning's n
1	Agriculture	0.050
2	Fresh water	0.025
3	Aquaculture	0.045
4	Estuarine water	0.025
6	Farmed wetlands	0.035
7	Estuarine emergent	0.050
8	Estuarine woody	0.140
9	Palustrine emergent	0.060
10	Bottomland hardwood	0.140
11	Riverine swamp	0.140
12	Pine savannah	0.090
13	Fresh water shrub/scrub	0.075
14	Palustrine non-vegetated	0.035
15	Transportation	0.032
16	High density urban	0.150
24	Urban fresh water	0.025
25	Wet soil/water/shadow	0.040
26	Urban pine	0.180
27	Urban hardwood	0.160
28	Urban low herbaceous	0.070
29	Urban grassy/pasture	0.055
30	Bare urban I	0.120
31	Bare urban II	0.120
32	Clear cuts	0.036
50	Low density pine	0.160
51	Medium density pine	0.180
52	High density pine	0.200
53	Medium density hardwood	0.170
54	High density hardwood	0.170
55	Mixed forest	0.160
56	Recent harvest	0.045
57	Cypress/tupelo	0.180
60	Agriculture	0.050
61	Grassy/pasture/range	0.050
62	Low herbaceous vegetation	0.050
63	Evergreen shrub	0.080
71	Wetland	0.050
80	Bare	0.035
81	Sand bar/beach	0.030

Table 4: Manning's n values for C-CAP classification.

C-CAP Class	Description	Manning's n
2	High intensity developed	0.120
3	Medium intensity developed	0.120
4	Low intensity developed	0.120
5	Developed open space	0.035
6	Cultivated land	0.100
7	Pasture/hay	0.050
8	Grassland	0.035
9	Deciduous forest	0.160
10	Evergreen forest	0.180
11	Mixed forest	0.170
12	Scrub/shrub	0.080
13	Palustrine forested wetland	0.150
14	Palustrine scrub/shrub wetland	0.075
15	Palustrine emergent wetland	0.060
16	Estuarine forested wetland	0.150
17	Estuarine scrub/shrub wetland	0.070
18	Estuarine emergent wetland	0.050
19	Unconsolidated shore	0.030
20	Bare land	0.030
21	Open water	0.025
22	Palustrine aquatic bed	0.035
23	Estuarine aquatic bed	0.030

Table 5: Summary of mean Scatter Index (*SI*) and mean normalized bias errors for the wave data sets. The mean errors for WAM and STWAVE are presented at all locations covered by their structured meshes. The mean errors for SWAN are presented at all locations, a sub-set of locations that are consistent with WAM/STWAVE, and a smaller sub-set without two NDBC buoys as indicated.

Data Set	Model	Locations	Number of Locations	Sign. Wave Height		Peak Wave Period		Mean Wave Period	
				<i>SI</i>	Bias	<i>SI</i>	Bias	<i>SI</i>	Bias
NDBC	WAM		9	0.26	0.09	0.25	0.10	0.15	0.11
	STWAVE		1	0.28	-0.07	0.26	0.02	0.16	-0.05
	WAM/STWAVE		10	0.26	0.07	0.25	0.09	0.15	0.09
	SWAN	All	12	0.32	0.15	0.29	0.04	0.17	-0.02
		Consistent Without 42019, 42020	10 8	0.31 0.26	0.14 0.12	0.26 0.22	0.03 -0.01	0.16 0.15	-0.02 -0.02
CSI	STWAVE		4	0.42	0.38	0.42	0.14	0.46	0.27
	SWAN	All	5	0.34	0.22	0.46	-0.07	0.35	-0.05
		Consistent	4	0.35	0.20	0.41	-0.05	0.37	-0.04
AK	STWAVE		8	0.31	0.38	0.40	0.15	--	--
	SWAN	All	16	0.31	0.28	0.45	-0.02	--	--
		Consistent	8	0.33	0.24	0.39	0.03	--	--
USACE-CHL	STWAVE		6	0.61	0.56	1.63	0.49	--	--
	SWAN		6	0.51	1.08	1.28	-0.19	--	--
All	WAM		9	0.26	0.09	0.25	0.10	0.15	0.11
	STWAVE		19	0.42	0.41	0.79	0.25	0.40	0.21
	WAM/STWAVE		28	0.37	0.31	0.61	0.20	0.32	0.14
	SWAN	All	39	0.34	0.35	0.53	-0.03	0.22	-0.03
		Consistent Without 42019, 42020	28 26	0.36 0.35	0.38 0.39	0.54 0.54	-0.03 -0.05	0.13 0.22	-0.03 -0.03

Table 6: Summary of errors for the ADCIRC water levels at all of the circulation data sets. The mean *SI* and mean normalized errors were computed only for the time series data, so there is no reported mean errors for the URS/FEMA HWM data set. The average absolute differences, average absolute error, and standard deviations have units of meters. The measurement errors require the HWM locations to be clustered geographically and hydraulically, and thus they could not be computed for five of the sparser data sets.

Data Set	Number of Locations	<i>SI</i>	Bias	Best Fit		ADCIRC to Measured HWMs		Measured HWMs		Estimated ADCIRC Errors	
				Slope	R^2	Avg Abs Diff	Std Dev	Avg Abs Diff	Std Dev	Avg Abs Error	Std Dev
CSI	5	0.37	0.19	0.904	0.622	0.238	0.303	--	--	--	--
AK	16	0.27	-0.04	0.882	0.828	0.149	0.171	0.030	0.049	0.119	0.164
NOAA	23	0.29	0.20	0.978	0.910	0.170	0.206	--	--	--	--
CHL	6	0.23	0.04	0.882	0.826	0.327	0.199	--	--	--	--
USACE	39	0.24	0.10	0.944	0.893	0.281	0.314	0.095	0.195	0.186	0.246
USGS (Perm)	18	0.19	0.09	1.038	0.830	0.184	0.241	--	--	--	--
USGS (Depl)	24	0.27	0.20	0.968	0.761	0.260	0.317	--	--	--	--
CRMS	232	0.23	0.15	0.969	0.704	0.177	0.223	0.049	0.097	0.128	0.201
FEMA	82	--	--	0.937	0.825	0.223	0.240	0.046	0.083	0.177	0.226
All	444	0.24	0.14	0.952	0.807	0.216	0.280	0.064	0.139	0.142	0.220

Figures

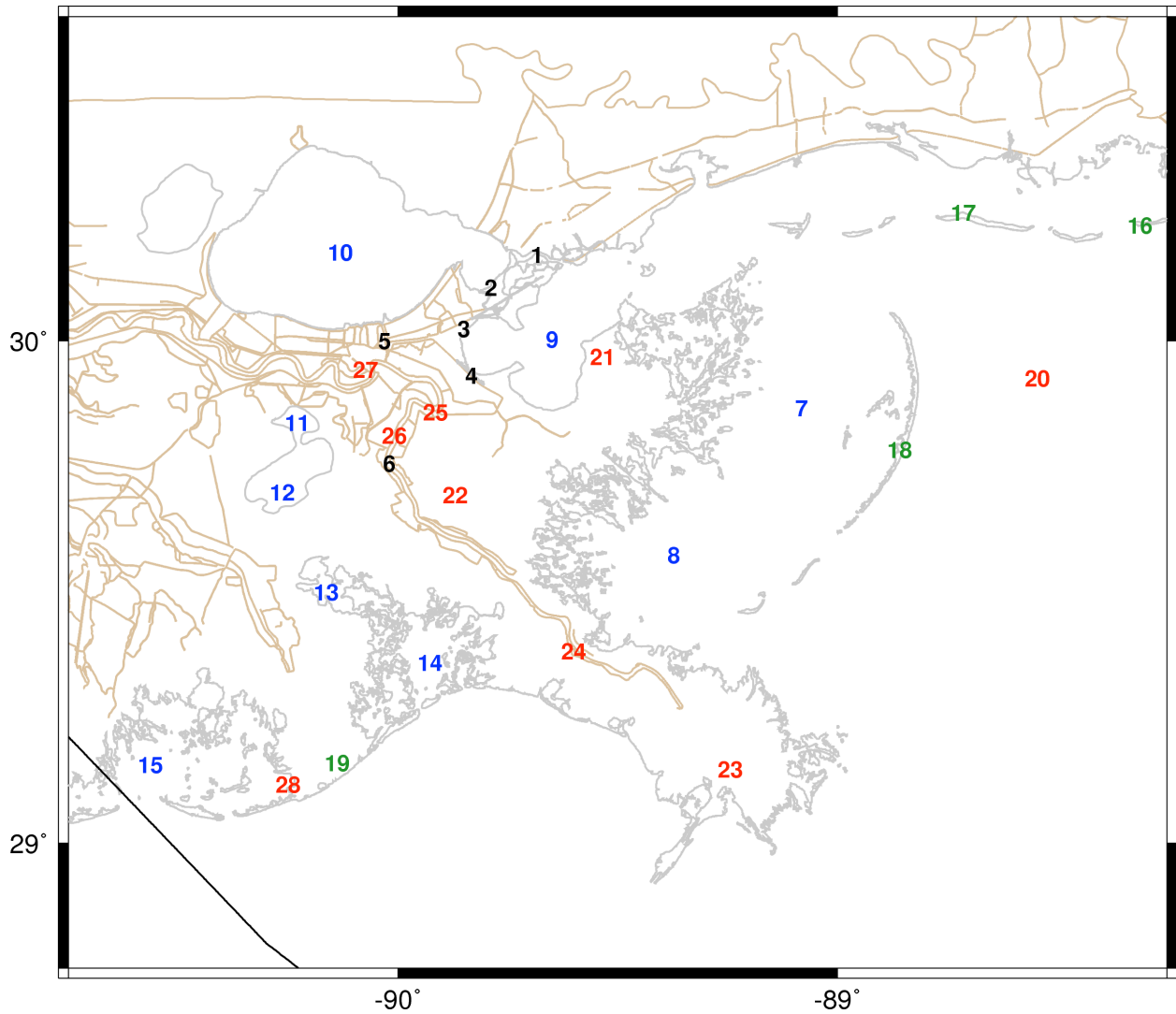


Figure 1: Schematic of southeastern Louisiana. Solid lines indicate Gustav's track (black), ADCIRC levee/road boundaries (brown) and the coastline (gray). Geographic locations of interest are indicated by numbers identified in Table 1.



Figure 2: Photographs during Gustav of (a) waves overtopping the IHNC walls near the Ninth Ward, and (b) surge overtopping the earthen levee near Braithwaite, courtesy of Nancy Powell, USACE.

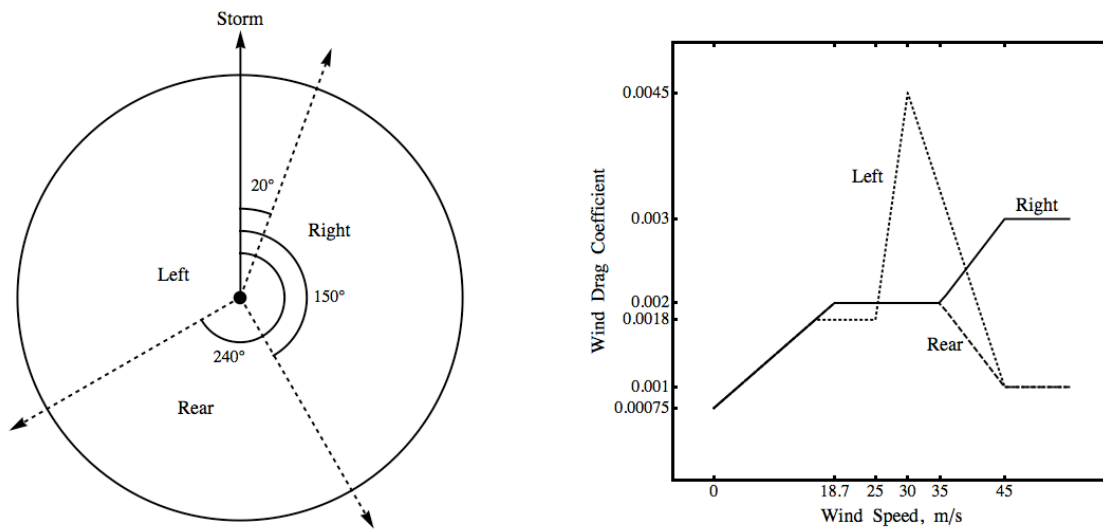


Figure 3: Schematics of the azimuthal wind drag, showing: extents of sectors in relation to direction of storm movement (left), and wind drag coefficient variability by storm sector (right), from Powell (2006).

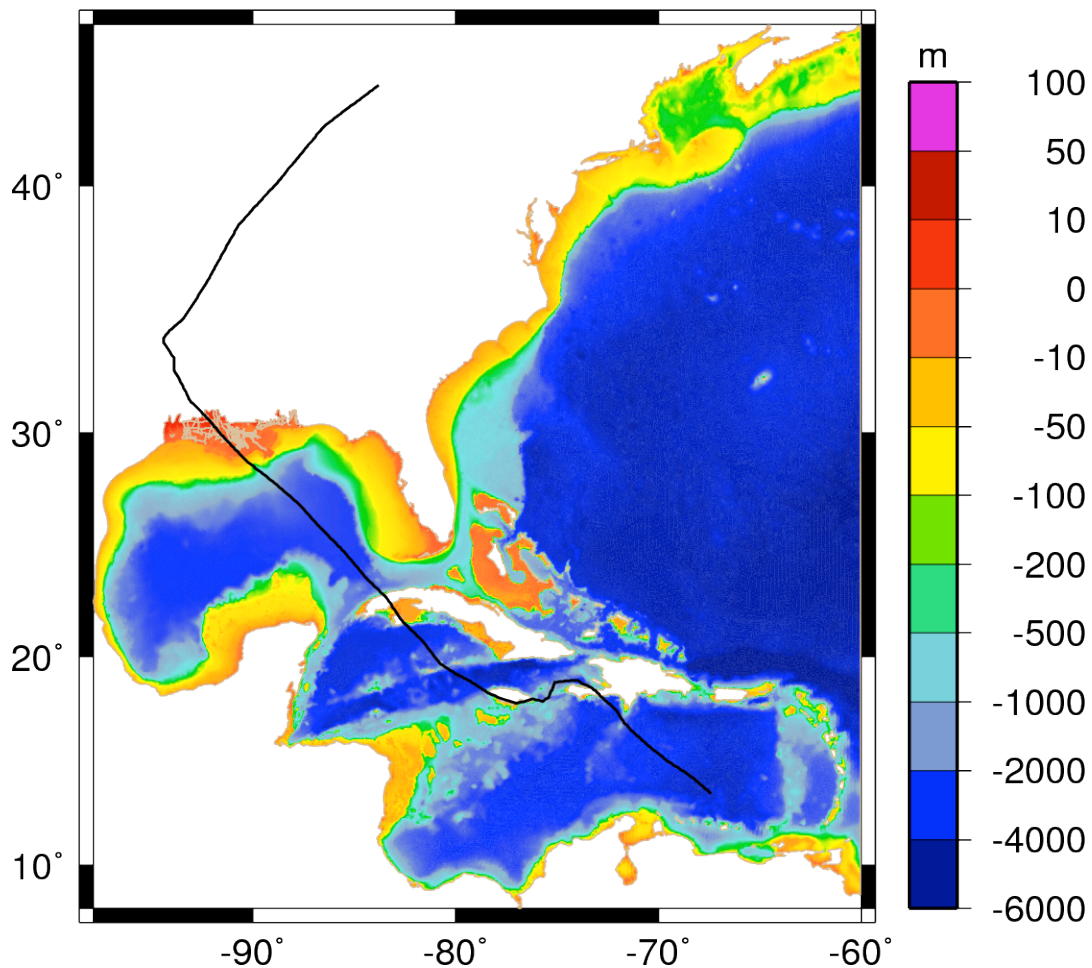


Figure 4: Bathymetry (m) of the SL16 mesh. Gustav's track is shown with a solid black line.

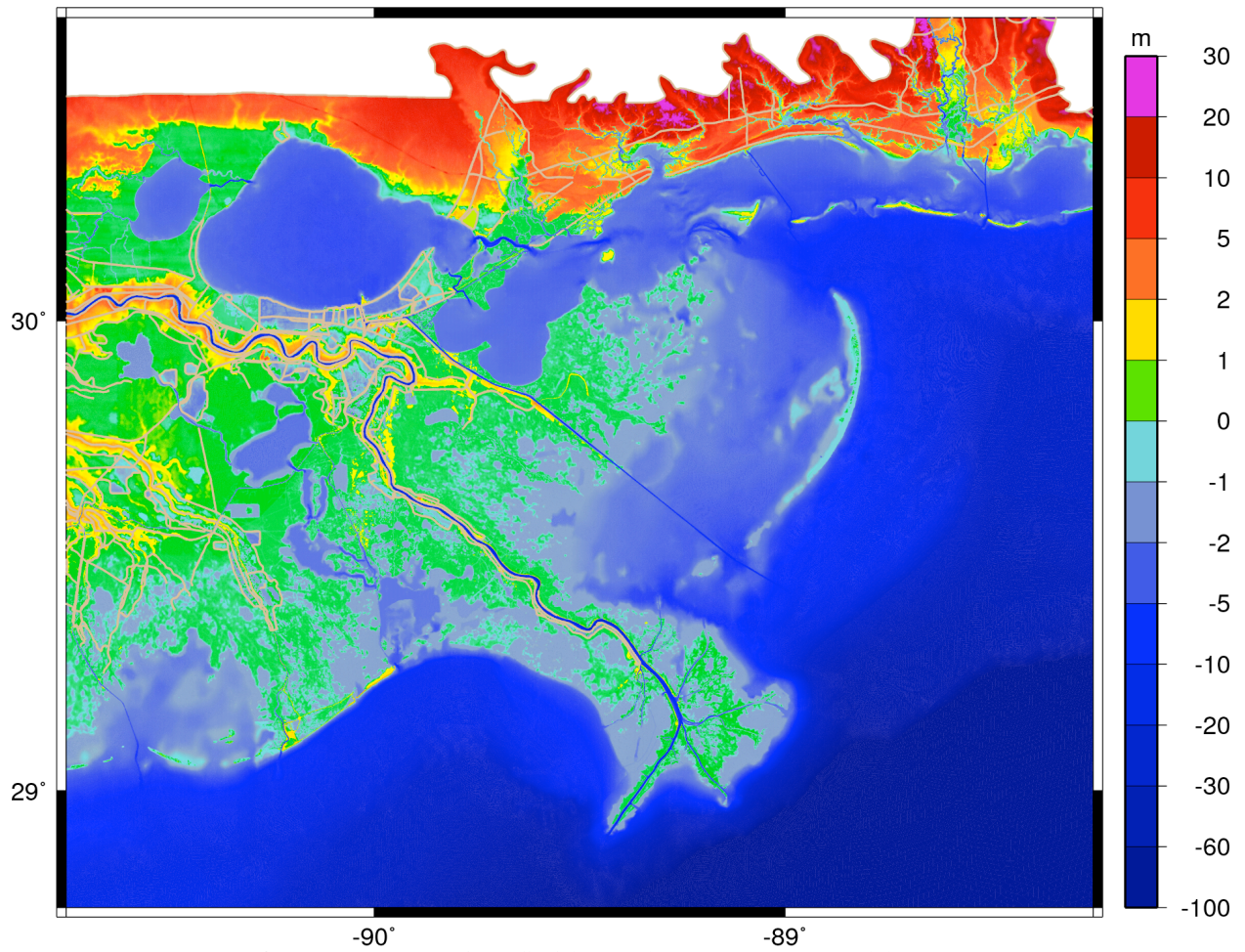


Figure 5: Bathymetry/topography (m) of the SL16 mesh in southeastern Louisiana.

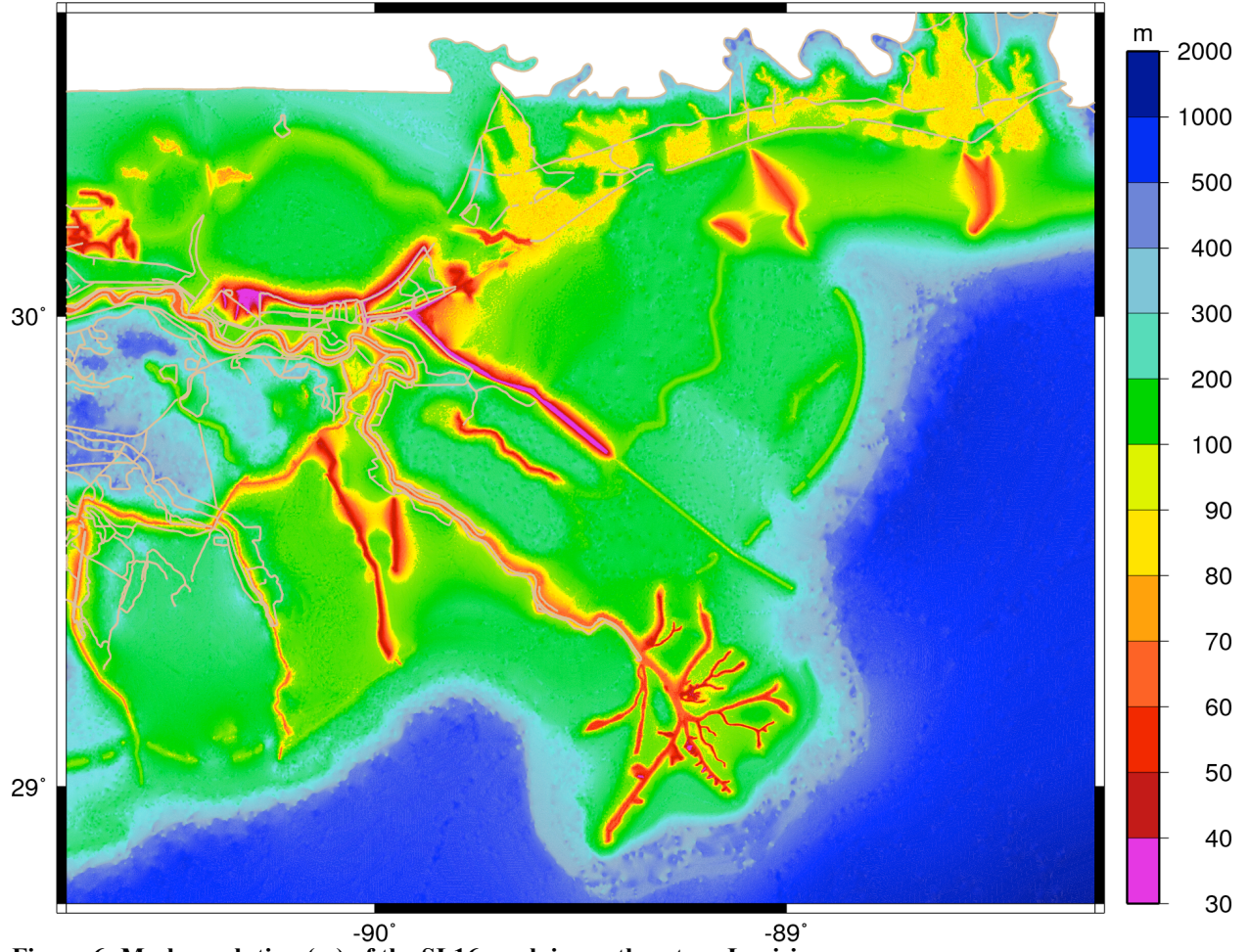


Figure 6: Mesh resolution (m) of the SL16 mesh in southeastern Louisiana.

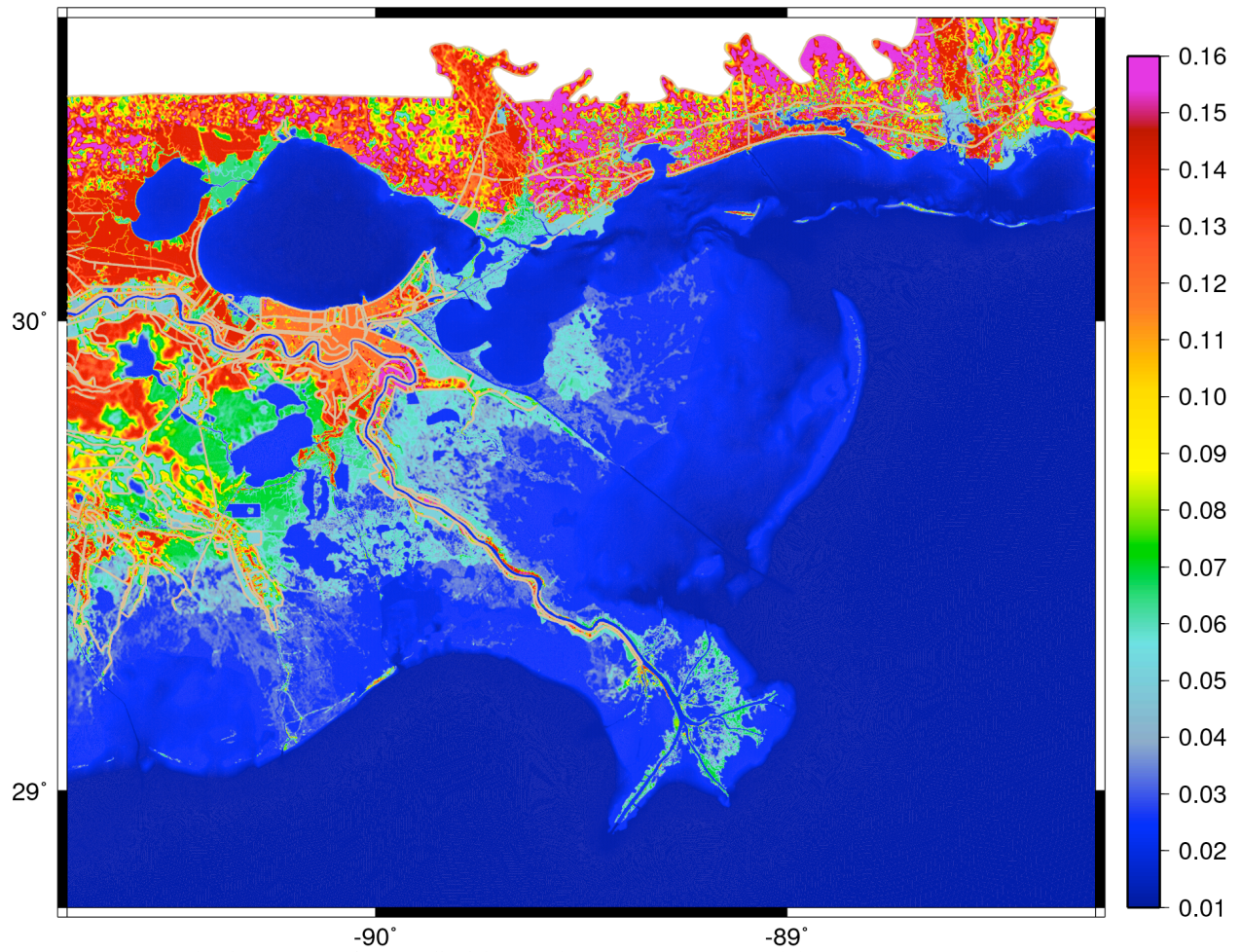


Figure 7: Manning's n values for the SL16 mesh in southeastern Louisiana.

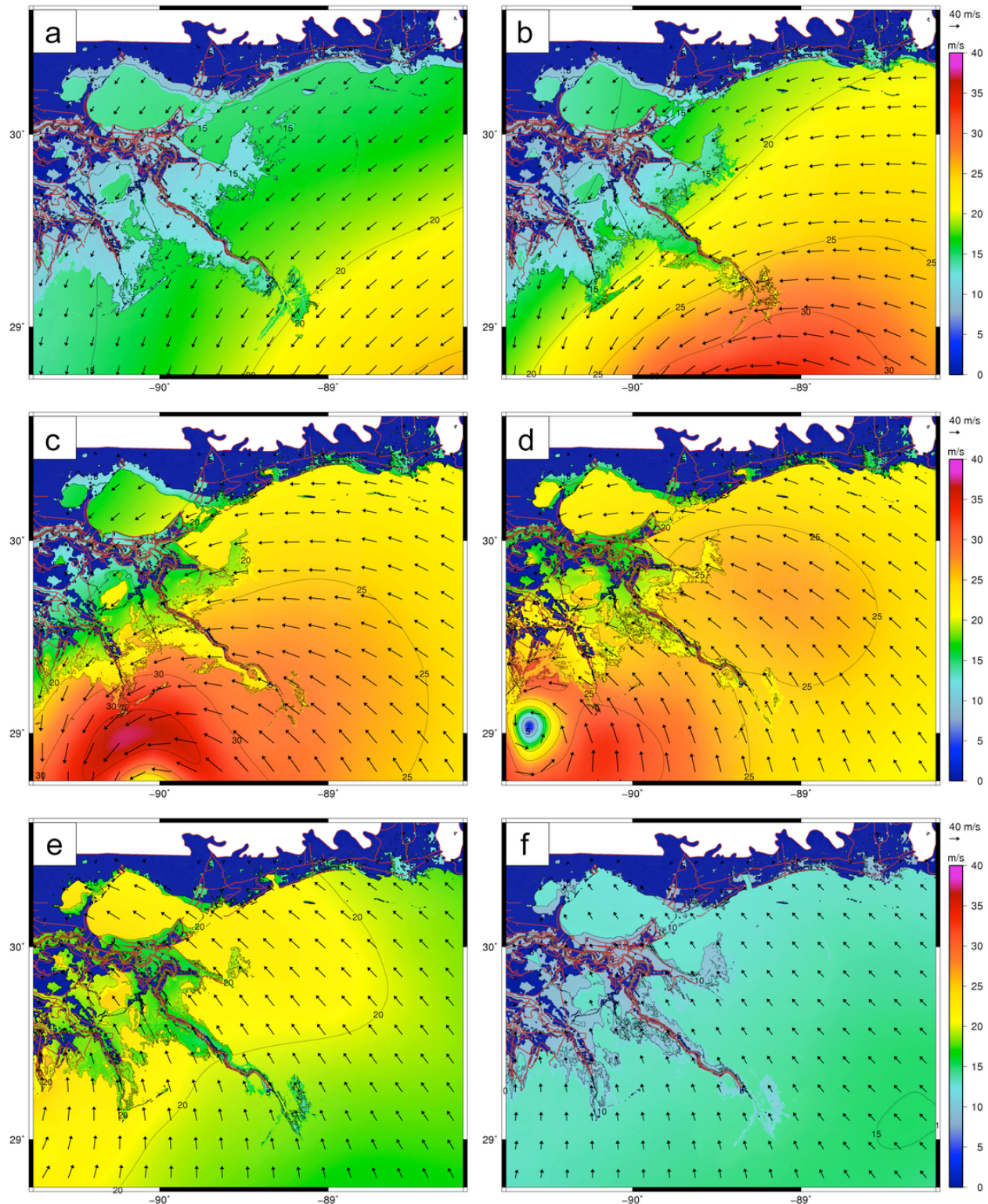


Figure 8: Wind speeds (m s^{-1}) in southeastern Louisiana during Hurricane Gustav. The panels correspond to the following times: (a) 0200 UTC 01 September 2008 or approximately 12hr before landfall, (b) 0800 UTC 01 September 2008 or approximately 6hr before landfall, (c) 1100 UTC 01 September 2008 or approximately 3hr before landfall, (d) 1400 UTC 01 September 2008 or approximately landfall, (e) 1700 UTC 01 September 2008 or approximately 3hr after landfall, (f) 0200 UTC 02 September 2008 or approximately 12hr after landfall.

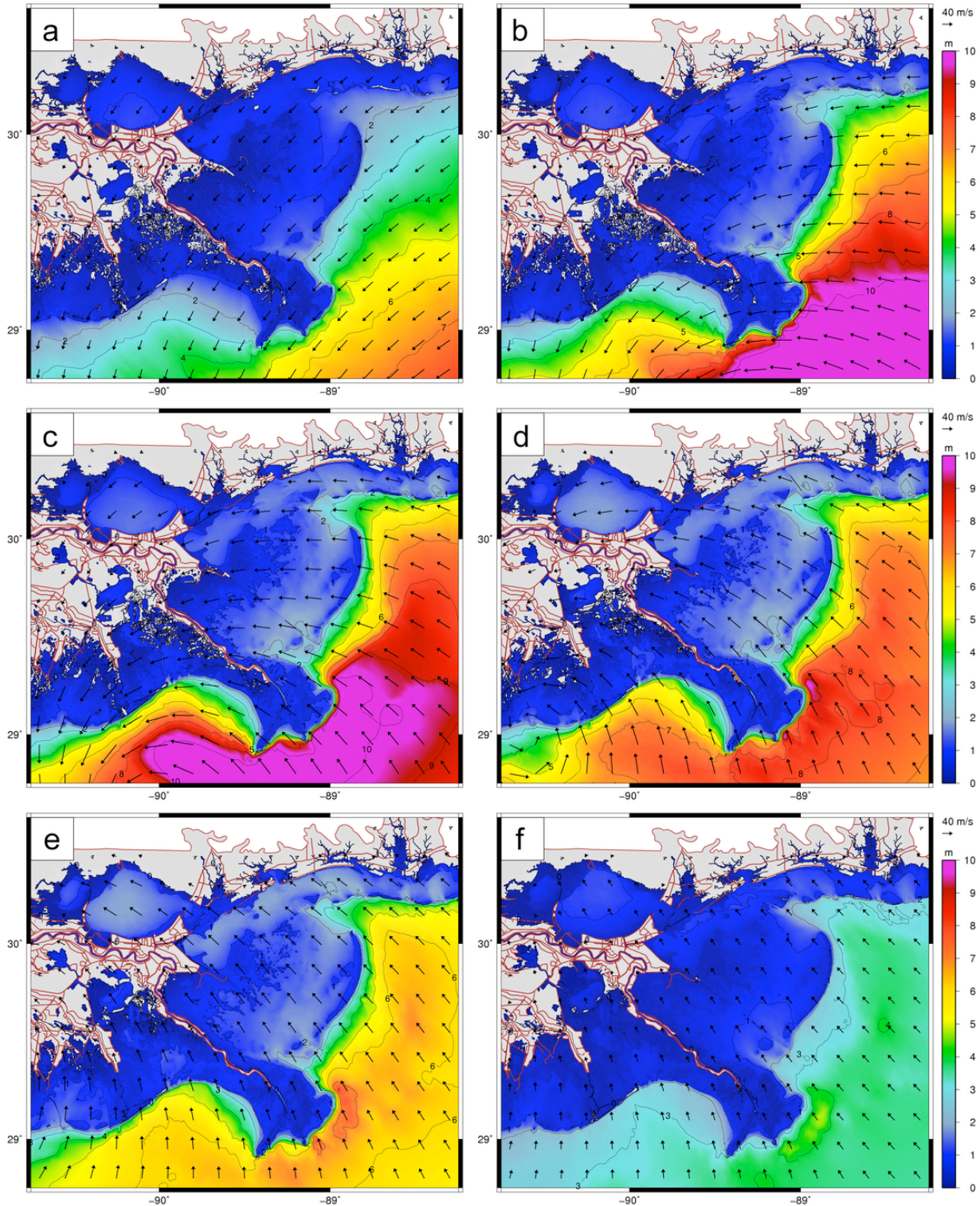


Figure 9: Contours of SWAN significant wave heights (m) and vectors of wind speeds (m s^{-1}) in southeastern Louisiana during Hurricane Gustav. The panels correspond to the following times: (a) 0200 UTC 01 September 2008 or approximately 12hr before landfall, (b) 0800 UTC 01 September 2008 or approximately 6hr before landfall, (c) 1100 UTC 01 September 2008 or approximately 3hr before landfall, (d) 1400 UTC 01 September 2008 or approximately landfall, (e) 1700 UTC 01 September 2008 or approximately 3hr after landfall, (f) 0200 UTC 02 September 2008 or approximately 12hr after landfall.

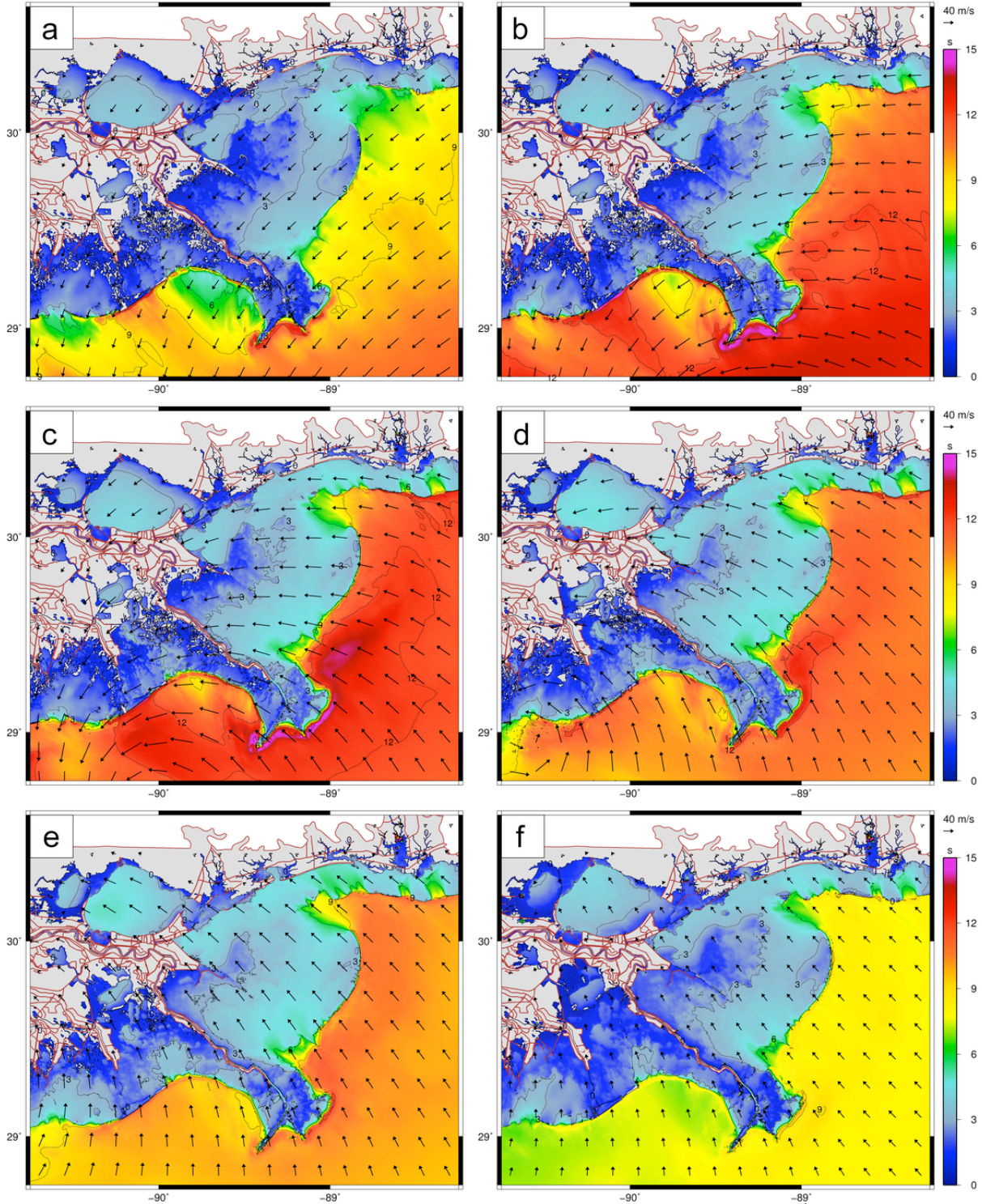


Figure 10: Contours of SWAN mean wave periods (s) and vectors of wind speeds (m s^{-1}) in southeastern Louisiana during Hurricane Gustav. The panels correspond to the following times: (a) 0200 UTC 01 September 2008 or approximately 12hr before landfall, (b) 0800 UTC 01 September 2008 or approximately 6hr before landfall, (c) 1100 UTC 01 September 2008 or approximately 3hr before landfall, (d) 1400 UTC 01 September 2008 or approximately landfall, (e) 1700 UTC 01 September 2008 or approximately 3hr after landfall, (f) 0200 UTC 02 September 2008 or approximately 12hr after landfall.

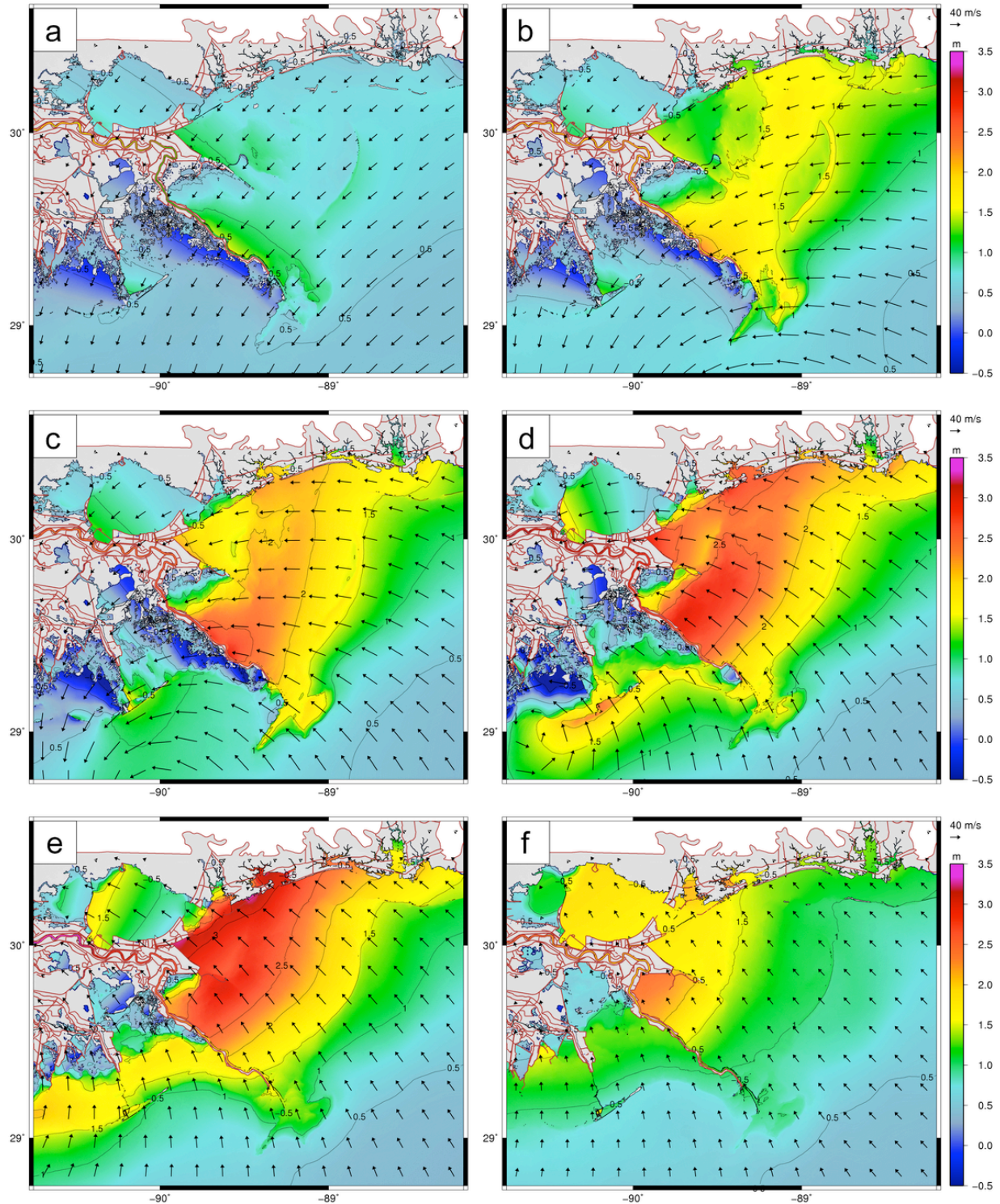


Figure 11: Contours of ADCIRC water levels (m relative to NAVD88 2004.65) and vectors of wind speeds (m s^{-1}) in southeastern Louisiana during Hurricane Gustav. The panels correspond to the following times: (a) 0200 UTC 01 September 2008 or approximately 12hr before landfall, (b) 0800 UTC 01 September 2008 or approximately 6hr before landfall, (c) 1100 UTC 01 September 2008 or approximately 3hr before landfall, (d) 1400 UTC 01 September 2008 or approximately landfall, (e) 1700 UTC 01 September 2008 or approximately 3hr after landfall, (f) 0200 UTC 02 September 2008 or approximately 12hr after landfall.

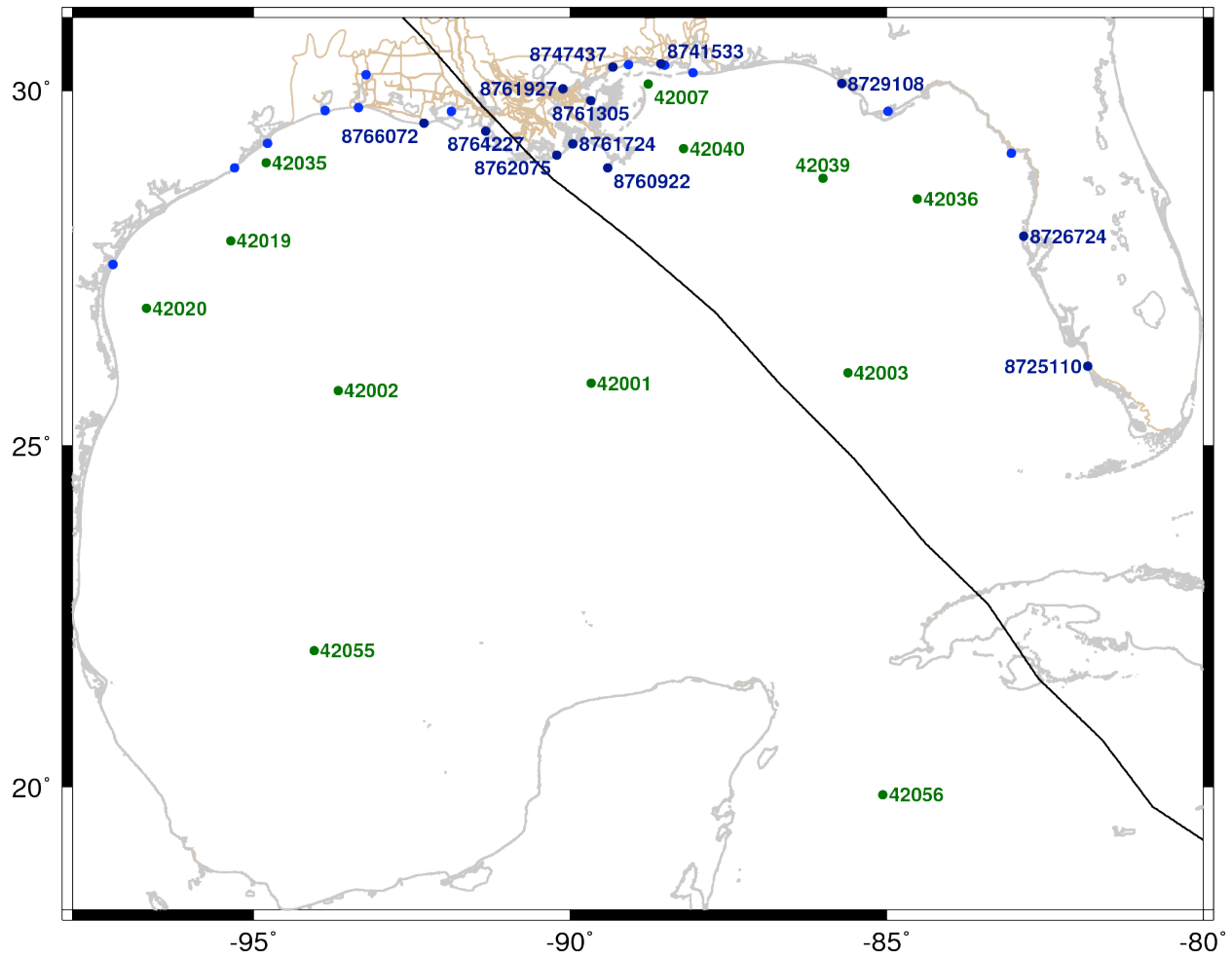


Figure 12: Locations of wave NDBC buoys (green points) and NOAA water level stations (blue points) in the Gulf of Mexico. The Gustav track is shown in black, the coastline and water bodies are shown in gray, and the boundaries of the SL16 mesh are shown in brown. Unlabeled NOAA water level stations are included in the analysis in Table 6, but their time series plots are not shown in Figure 21.

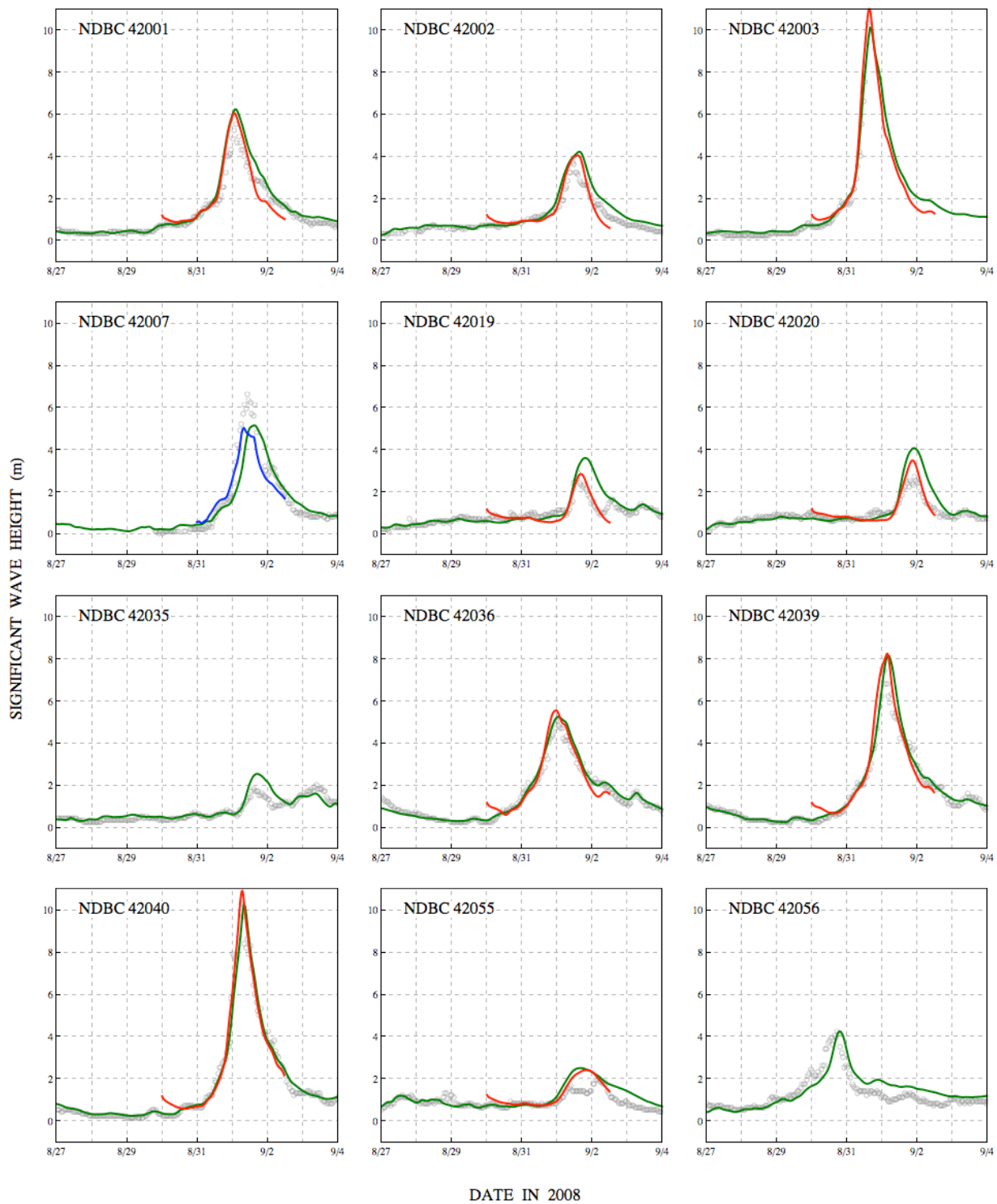


Figure 13: Time series of significant wave heights (m) at the 12 NDBC buoys shown in Figure 12. Measured NDBC values are shown with gray circles, while modeled results from SWAN (green), WAM (red) and STWAVE (blue) are shown with solid lines. Buoy 42003 stopped recording as the storm passed.

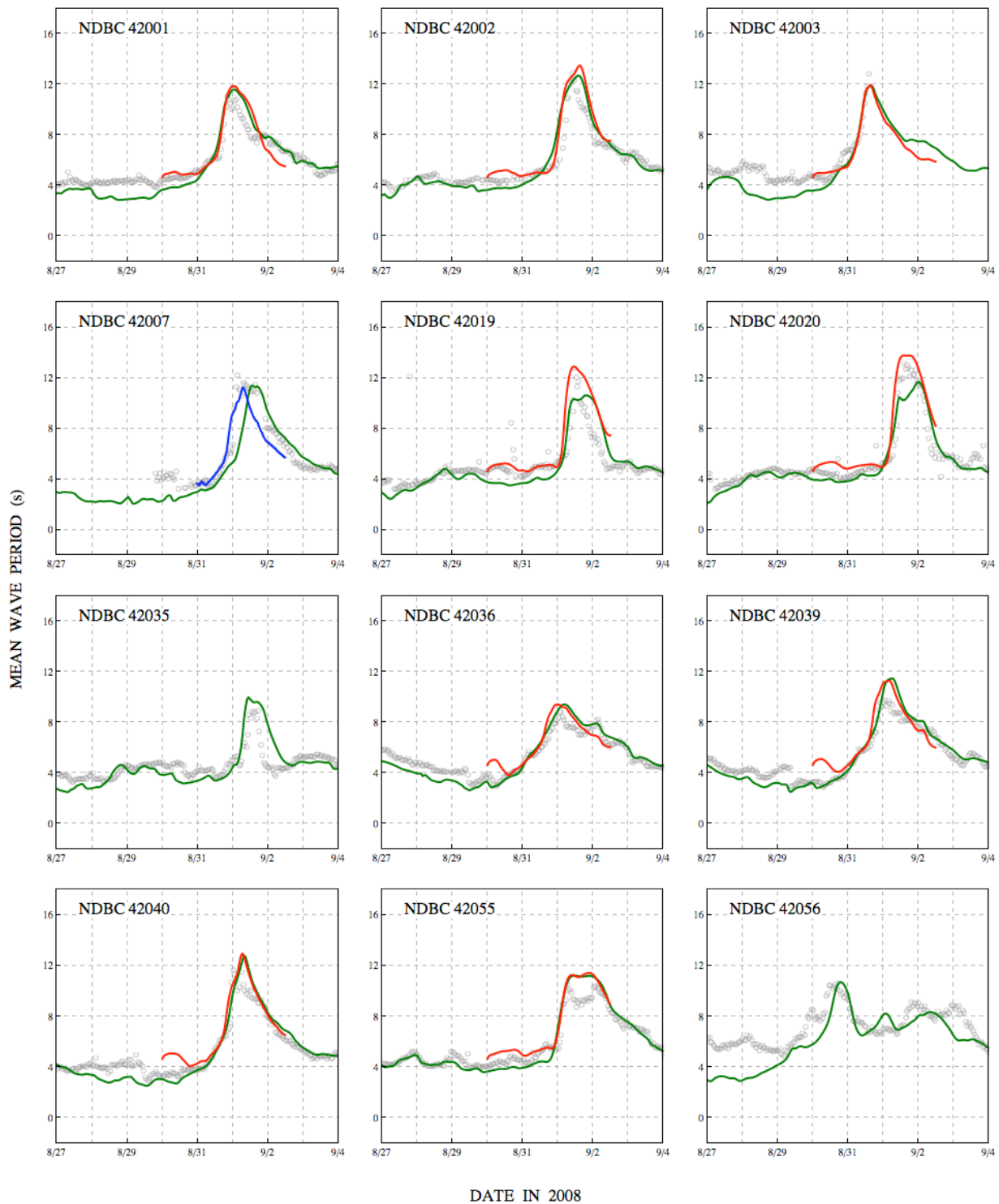


Figure 14: Time series of mean periods (s) at the 12 NDBC buoys shown in Figure 12. Measured NDBC values are shown with gray circles, while modeled results from SWAN (green), WAM (red) and STWAVE (blue) are shown with solid lines. Buoy 42003 stopped recording as the storm passed.

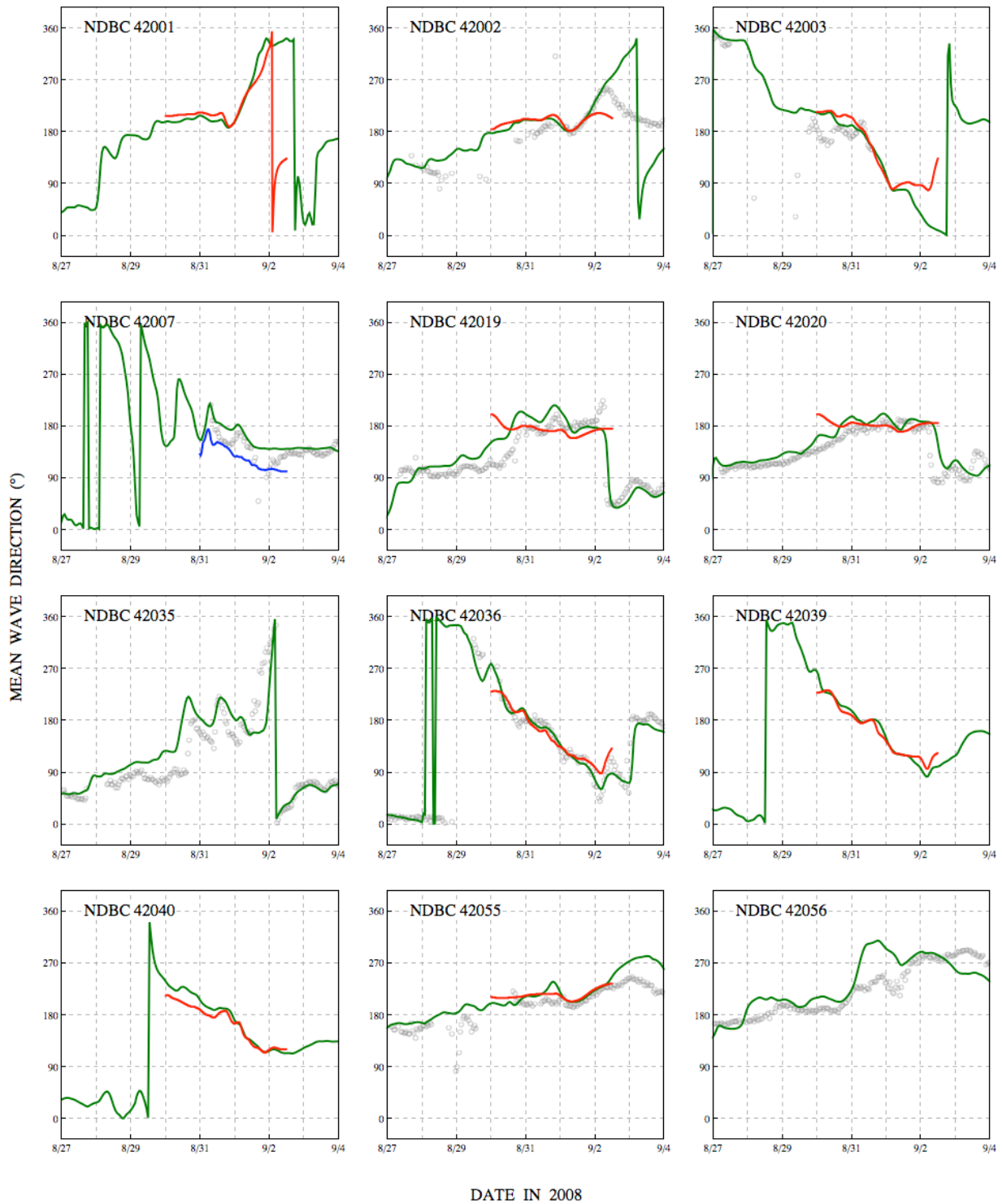


Figure 15: Time series of mean directions (°) at the 12 NDBC buoys shown in Figure 12. Measured NDBC values are shown with gray circles, while modeled results from SWAN (green), WAM (red) and STWAVE (blue) are shown with solid lines. Buoy 42003 stopped recording as the storm passed.

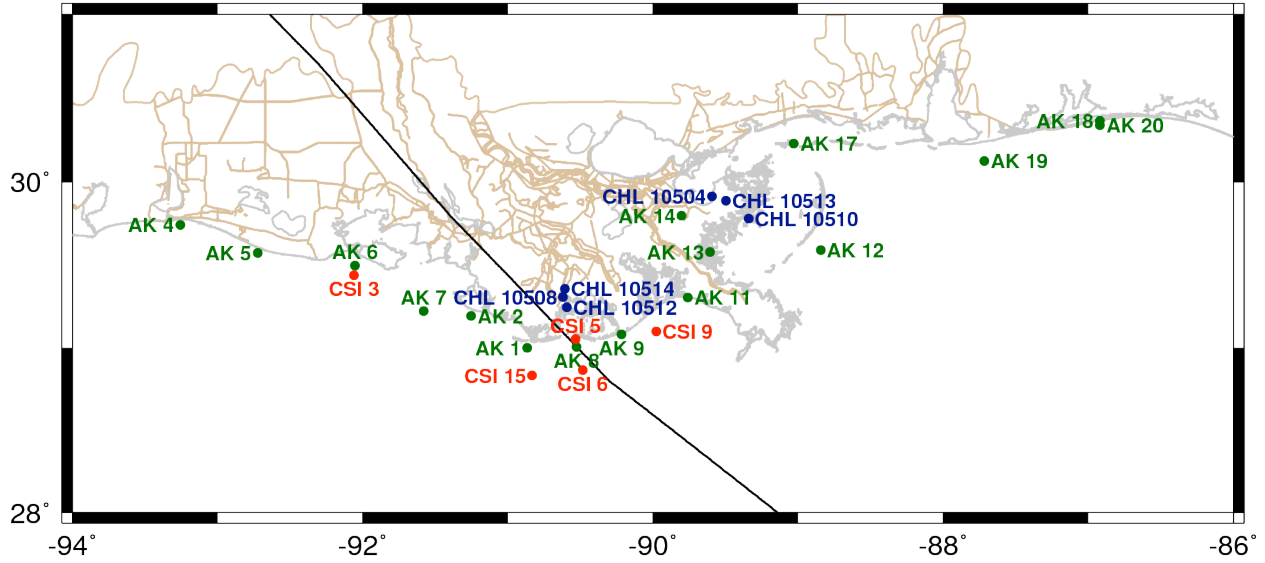


Figure 16: Locations of the nearshore AK gages (green points), CHL gages (blue points) and CSI stations (red points) in the northern Gulf of Mexico. The Gustav track is shown in black, the coastline and water bodies are shown in gray, and the boundaries of the SL16 mesh are shown in brown.

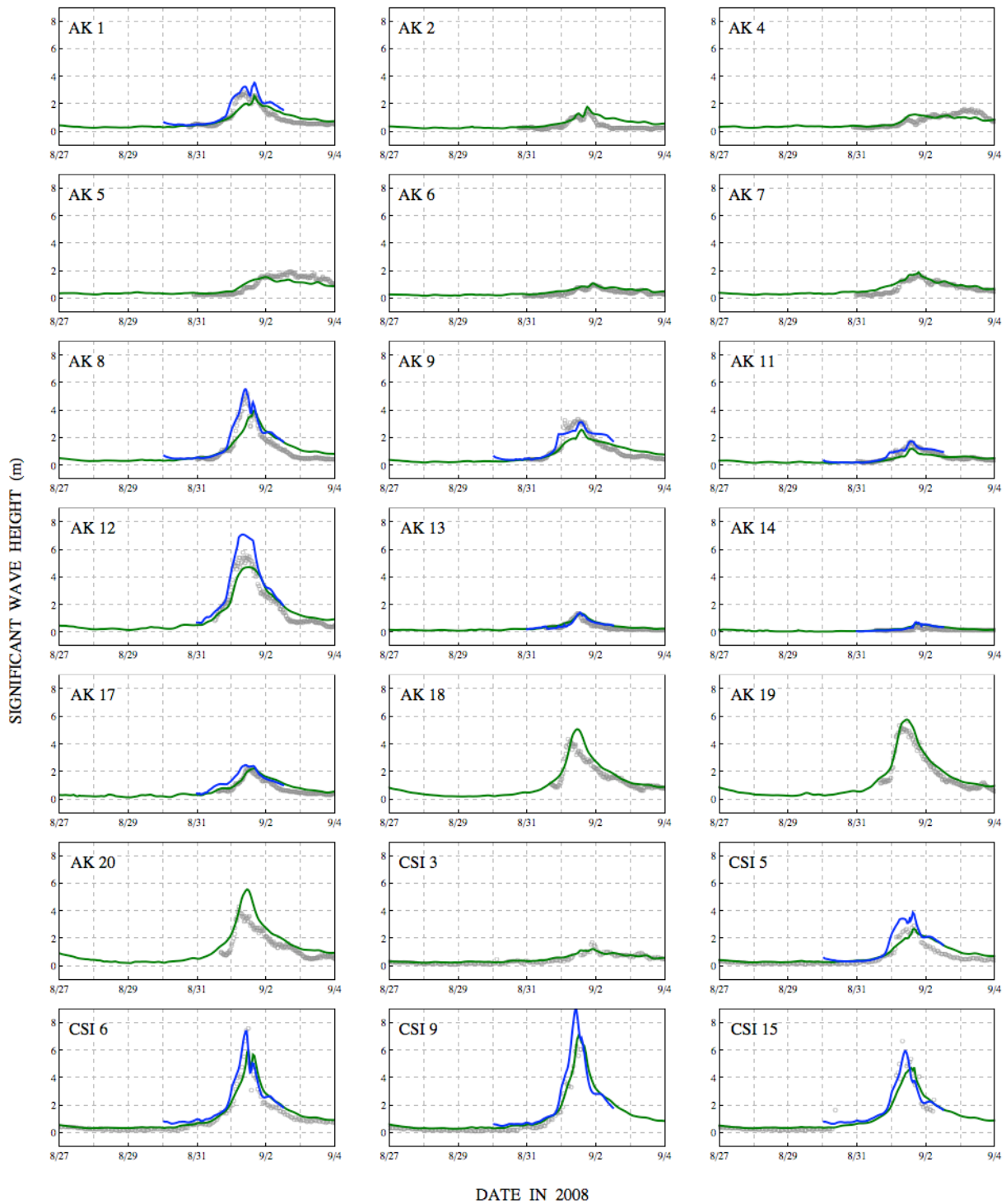


Figure 17. Time series of significant wave heights (m) at the 16 AK gages and five CSI gages shown in Figure 16. Measured values are shown with gray circles, modeled results from SWAN (green) and STWAVE (blue) are shown with solid lines.

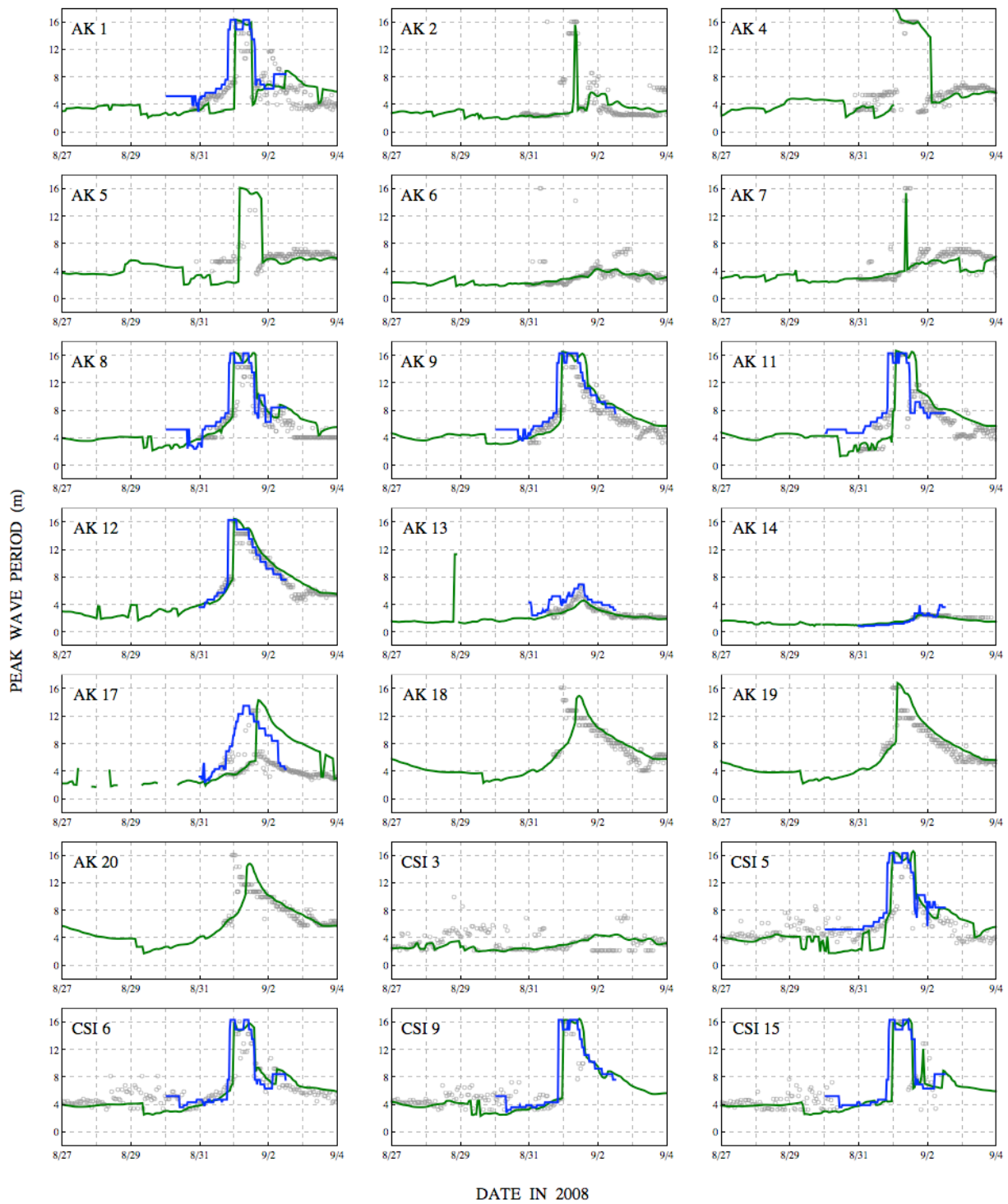


Figure 18: Time series of peak wave periods (s) at the 16 AK gages and five CSI gages shown in Figure 16. Measured values are shown with gray circles, modeled results from SWAN (green) and STWAVE (blue) are shown with solid lines.

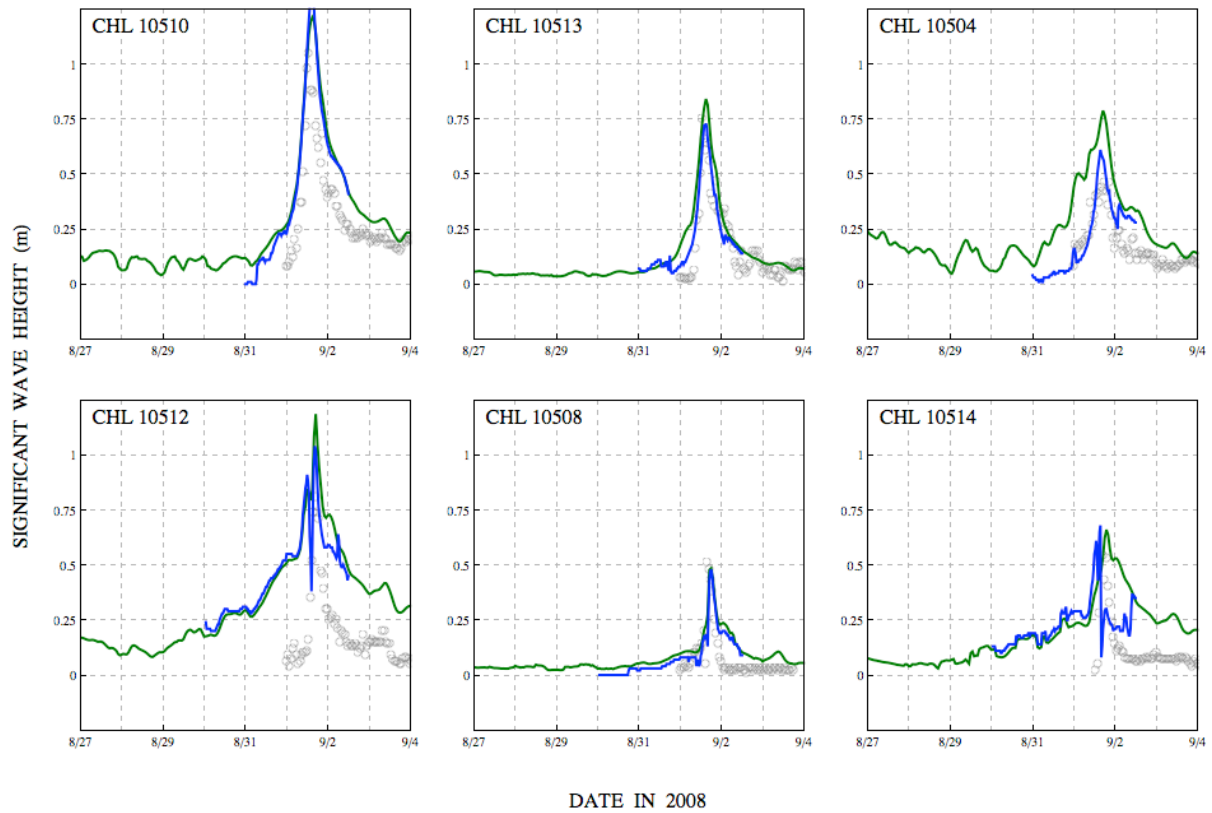


Figure 19: Time series of significant wave heights (m) at the six CHL gages shown in Figure 16. Measured values are shown with gray circles, modeled results from SWAN (green) and STWAVE (blue) are shown with solid lines.

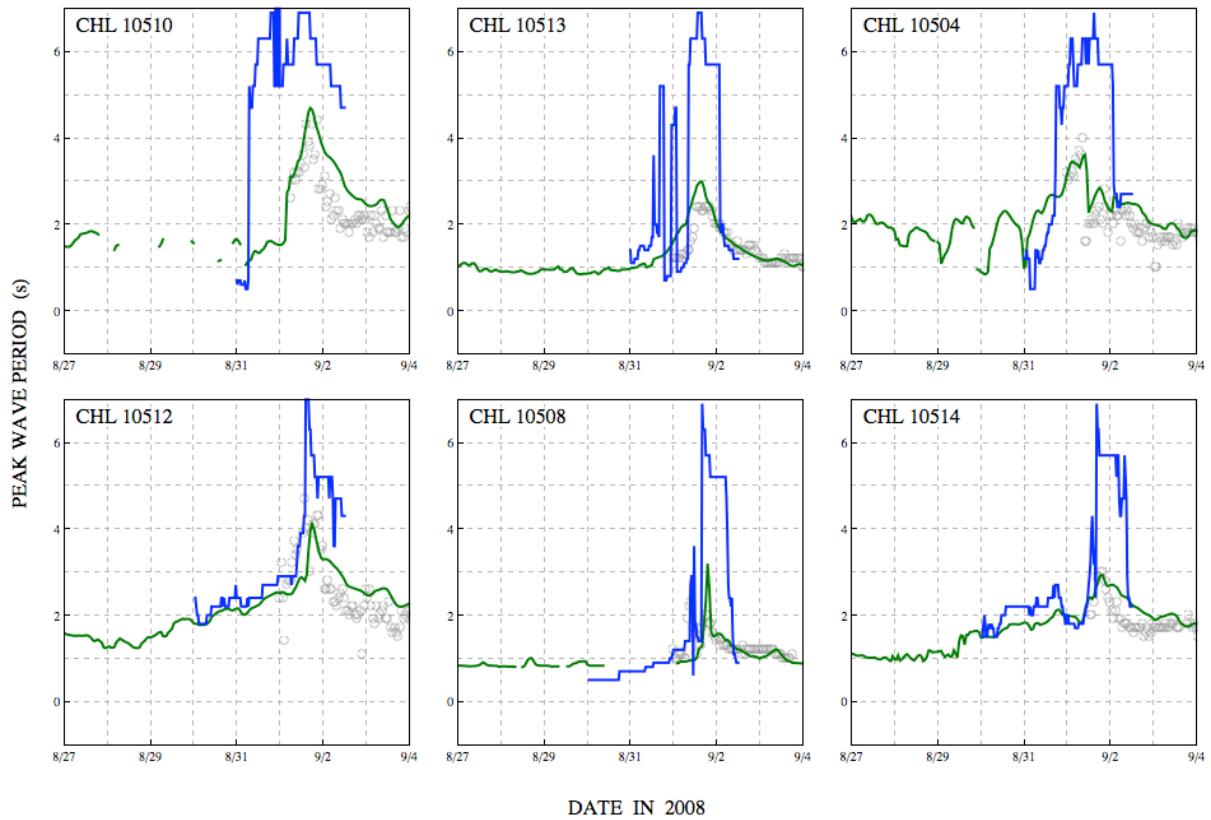


Figure 20: Time series of peak wave periods (s) at the six CHL gages shown in Figure 16. Measured values are shown with gray circles, modeled results from SWAN (green) and STWAVE (blue) are shown with solid lines.

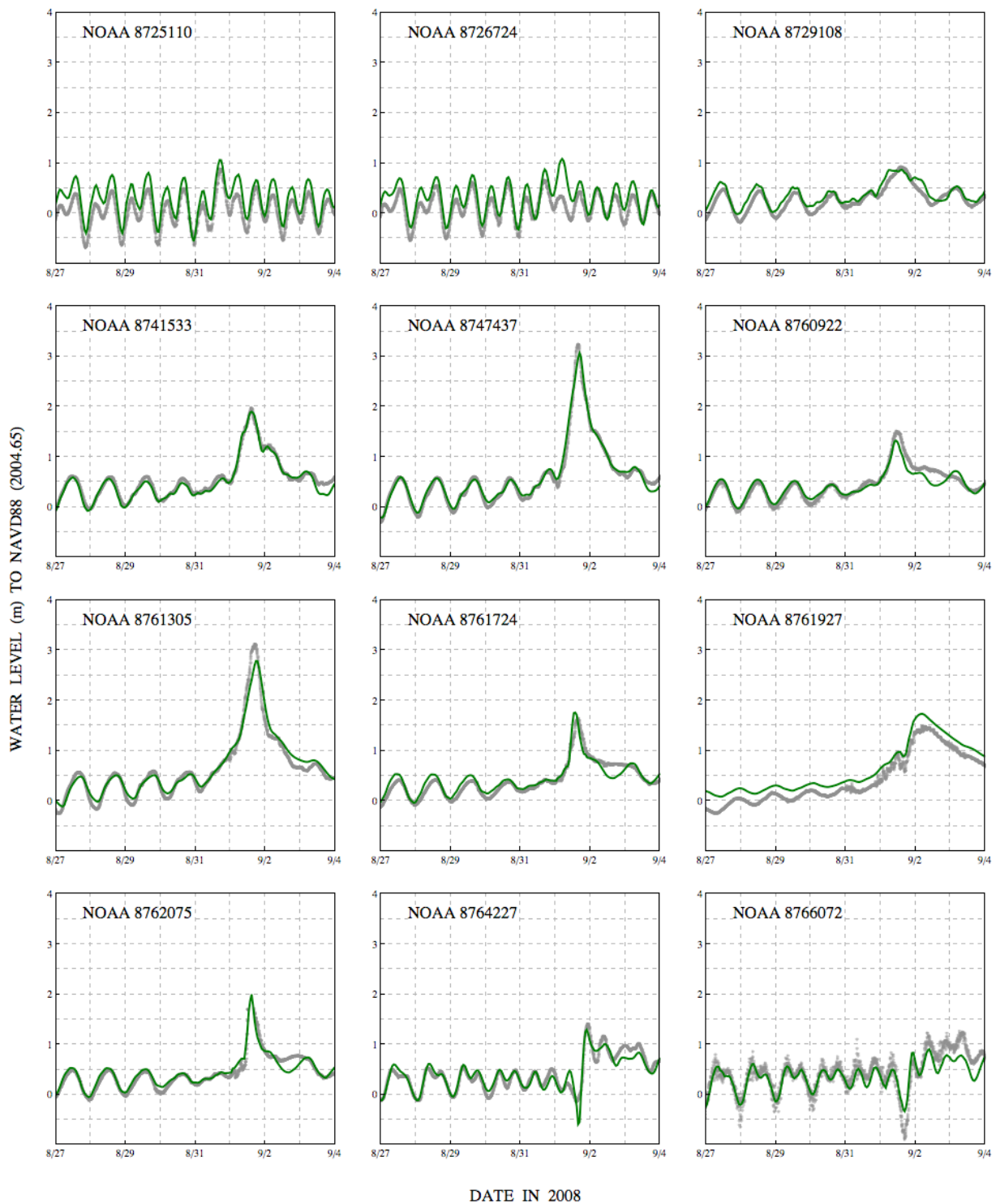


Figure 21: Time series of water levels (m relative to NAVD88 2004.65) at the 12 selected NOAA stations labeled in Figure 12. Measured NOAA values are shown with gray circles, and modeled ADCIRC results are shown with a green line.

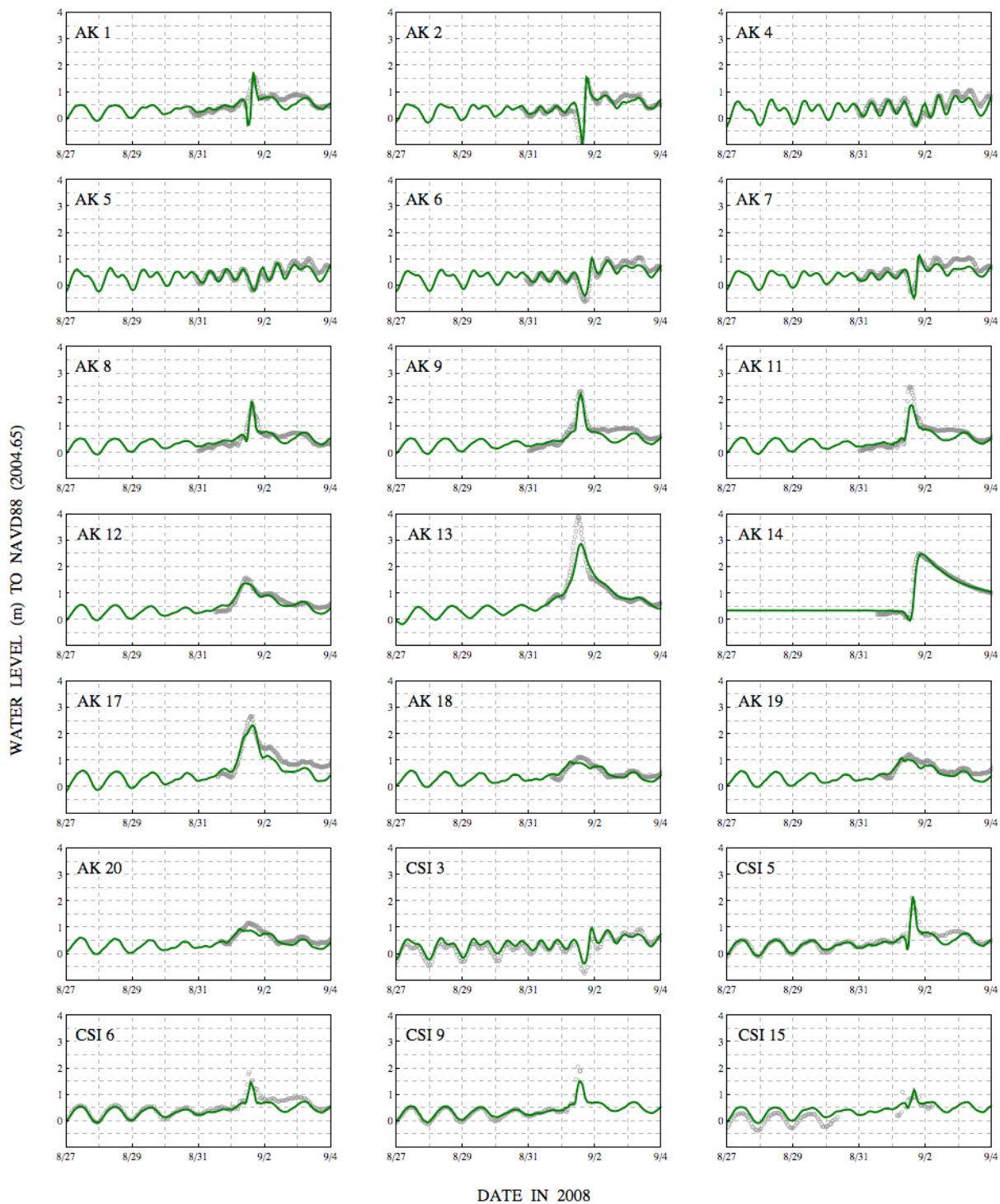


Figure 22: Time series of water levels (m relative to NAVD88 2004.65) at the 16 AK gages and five CSI gages shown in Figure 16. Measured values are shown with gray circles, and modeled ADCIRC results are shown with a green line.

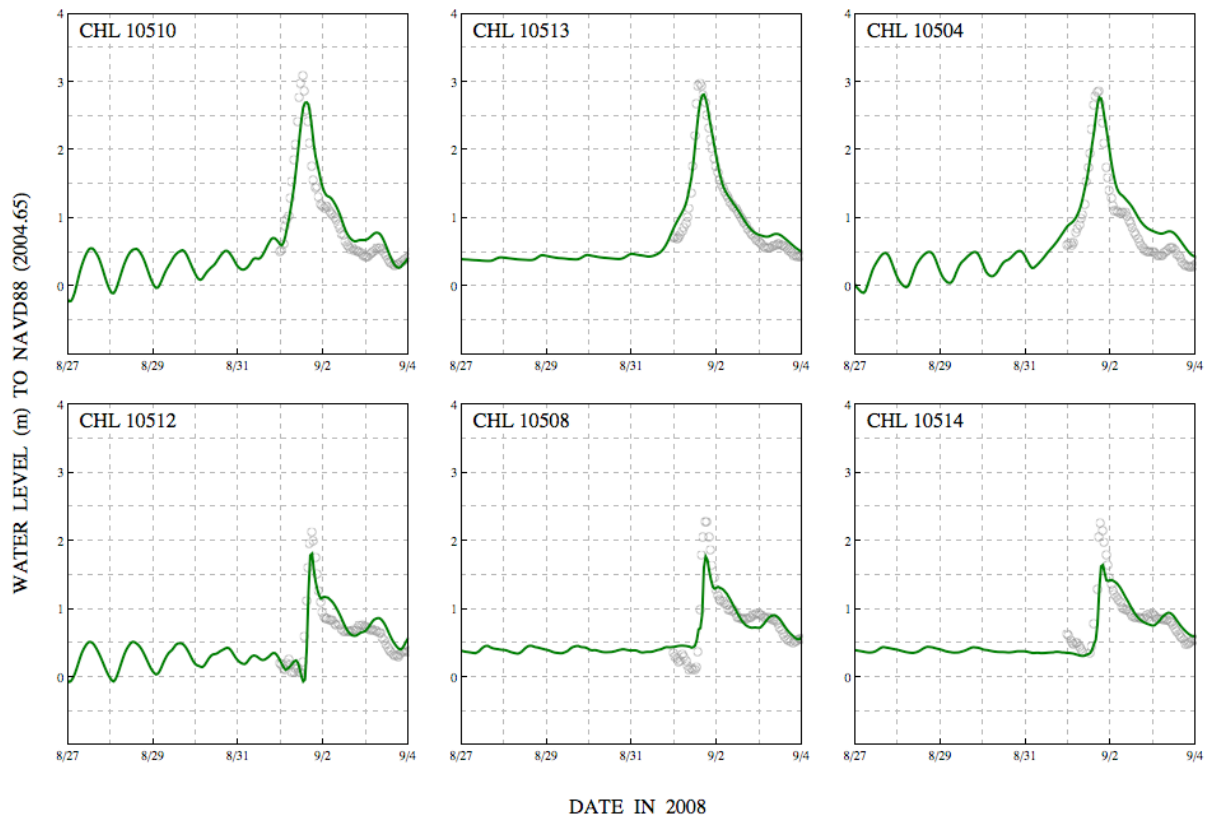


Figure 23: Time series of water levels (m relative to NAVD88 2004.65) at the six CHL gages shown in Figure 16. Measured values are shown with gray circles, and modeled ADCIRC results are shown with a green line.

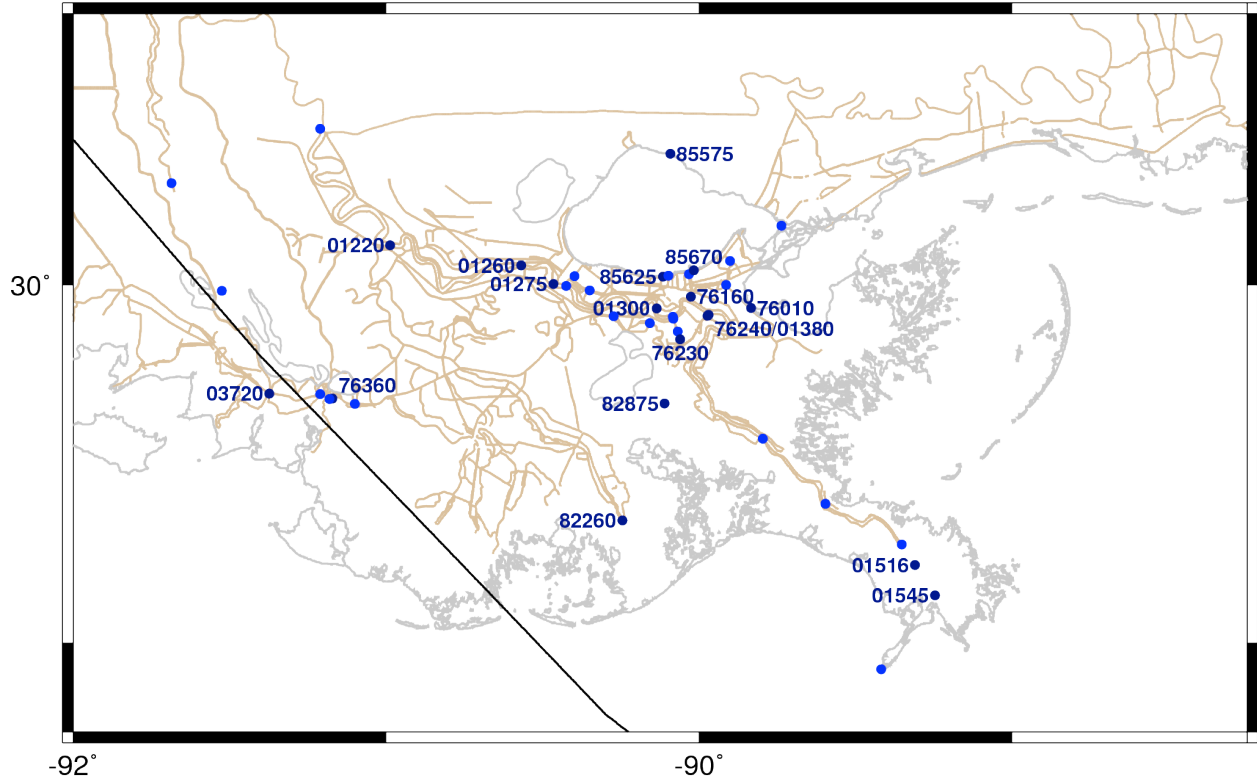


Figure 24: Locations of the USACE water level stations (blue points) in southeastern Louisiana. The Gustav track is shown in black, the coastline and water bodies are shown in gray, and the boundaries of the SL16 mesh are shown in brown. Unlabeled USACE stations are included in the analysis in Table 6, but their time series plots are not shown in Figure 25.

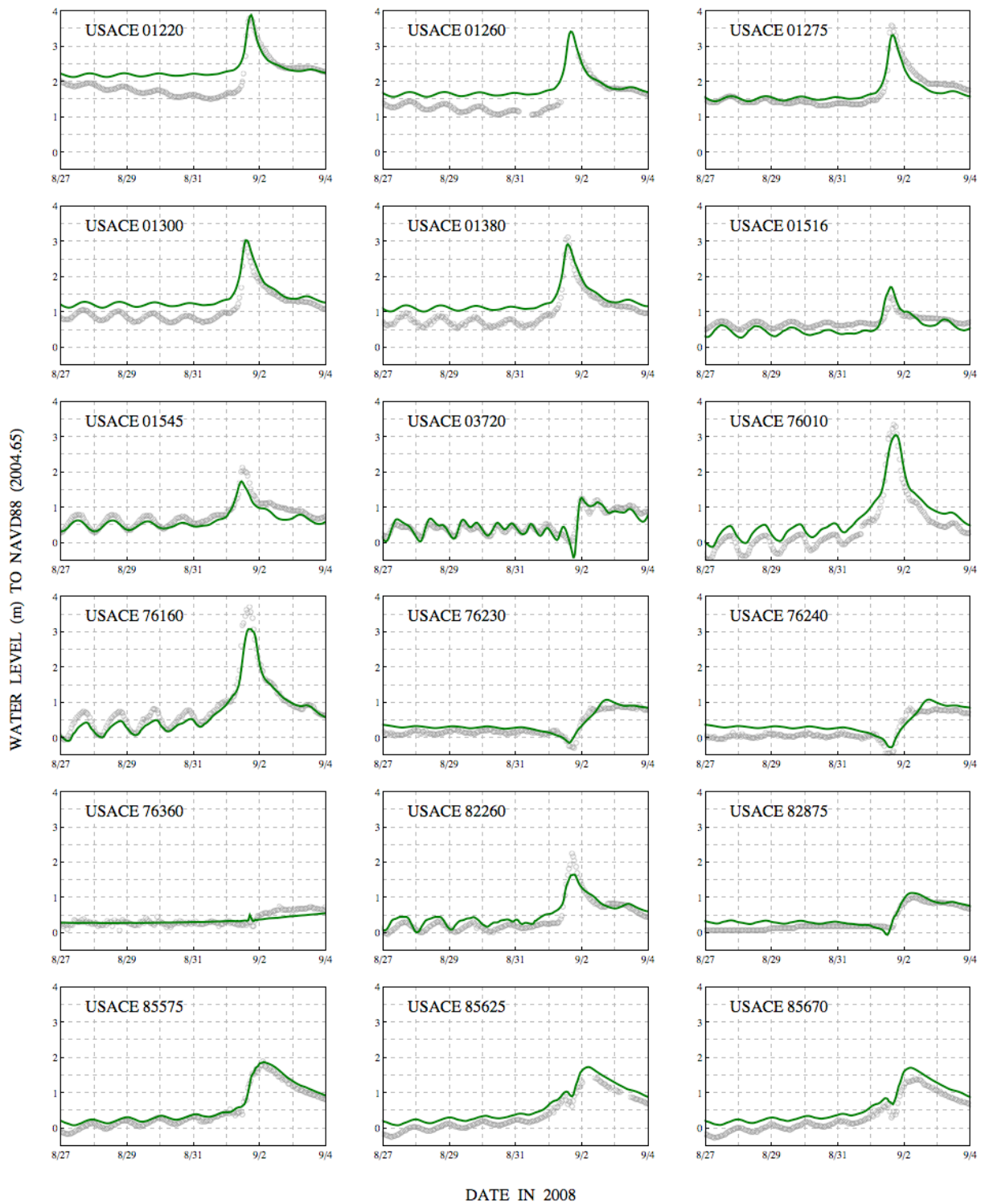


Figure 25: Time series of water levels (m relative to NAVD88 2004.65) at the 18 selected USACE stations labeled in Figure 24. Measured USACE values are shown with gray circles, while modeled ADCIRC results are shown with a green line.

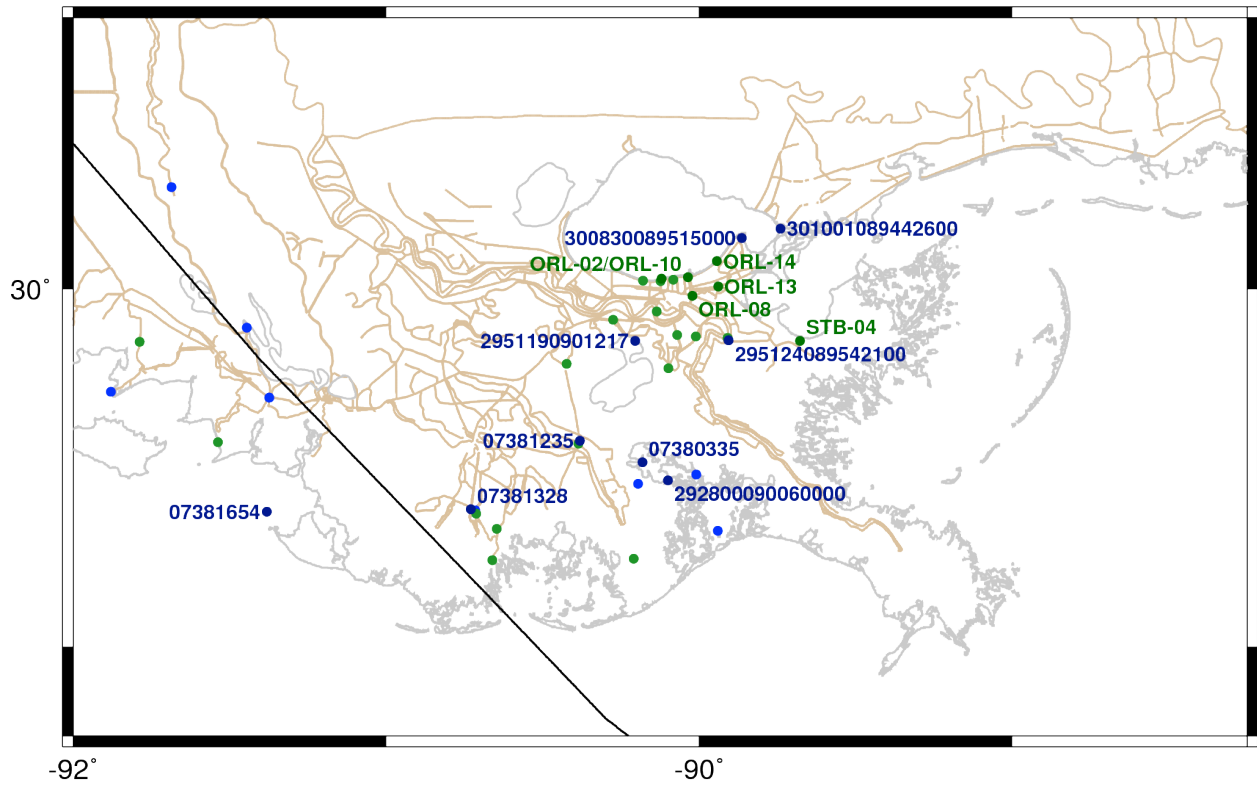


Figure 26: Locations of the permanent USGS water level stations (blue points) and deployable USGS water level gages (green points) in southeastern Louisiana. The Gustav track is shown in black, the coastline and water bodies are shown in gray, and the boundaries of the SL16 mesh are shown in brown. Unlabeled USGS stations are included in the analysis in Table 6, but their time series plots are not shown in Figure 27.

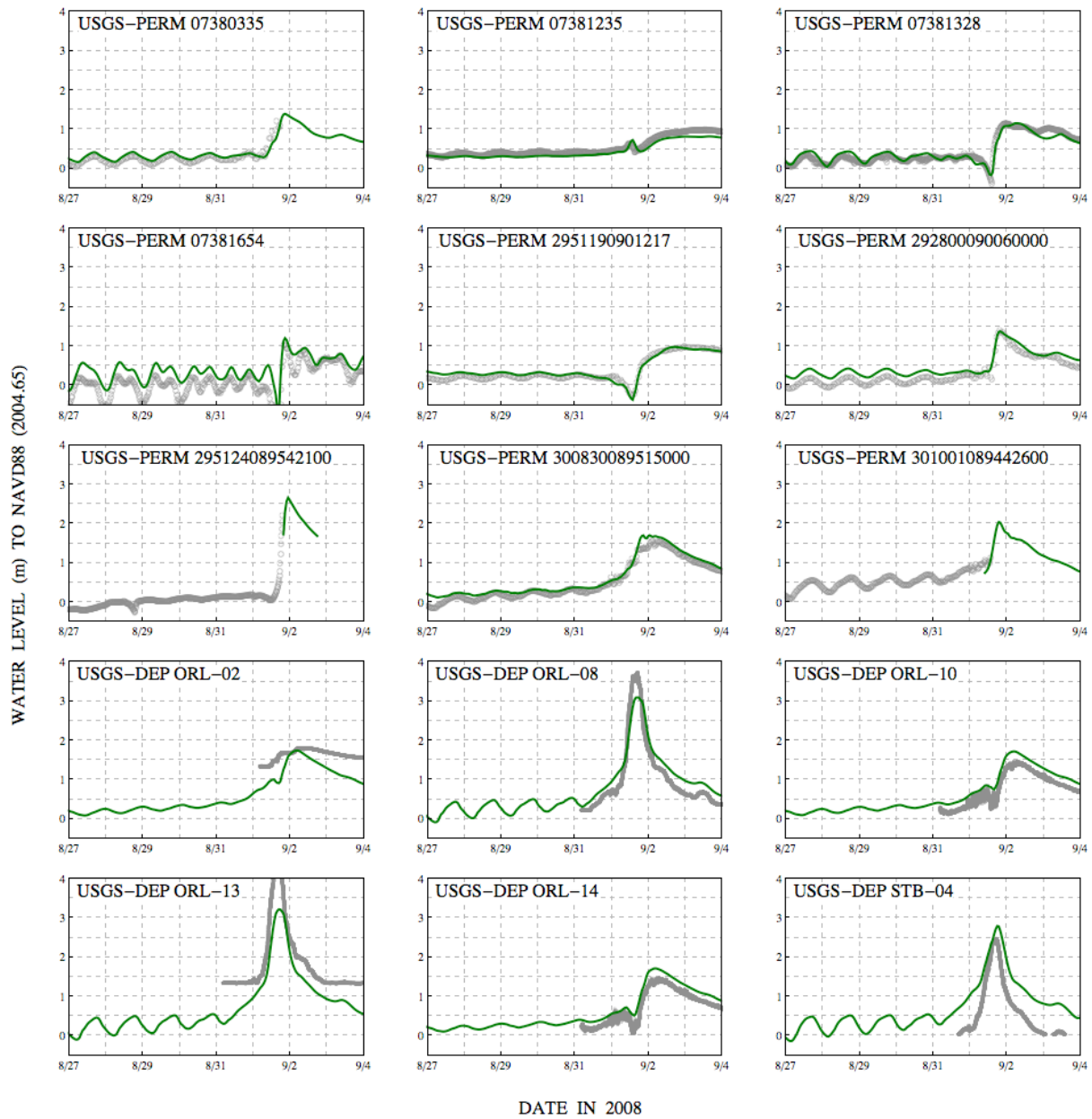


Figure 27: Time series of water levels (m relative to NAVD88 2004.65) at the selected nine permanent USGS stations and six deployable USGS gages labeled in Figure 26. Measured USGS values are shown with gray circles, and modeled ADCIRC results are shown with a green line.

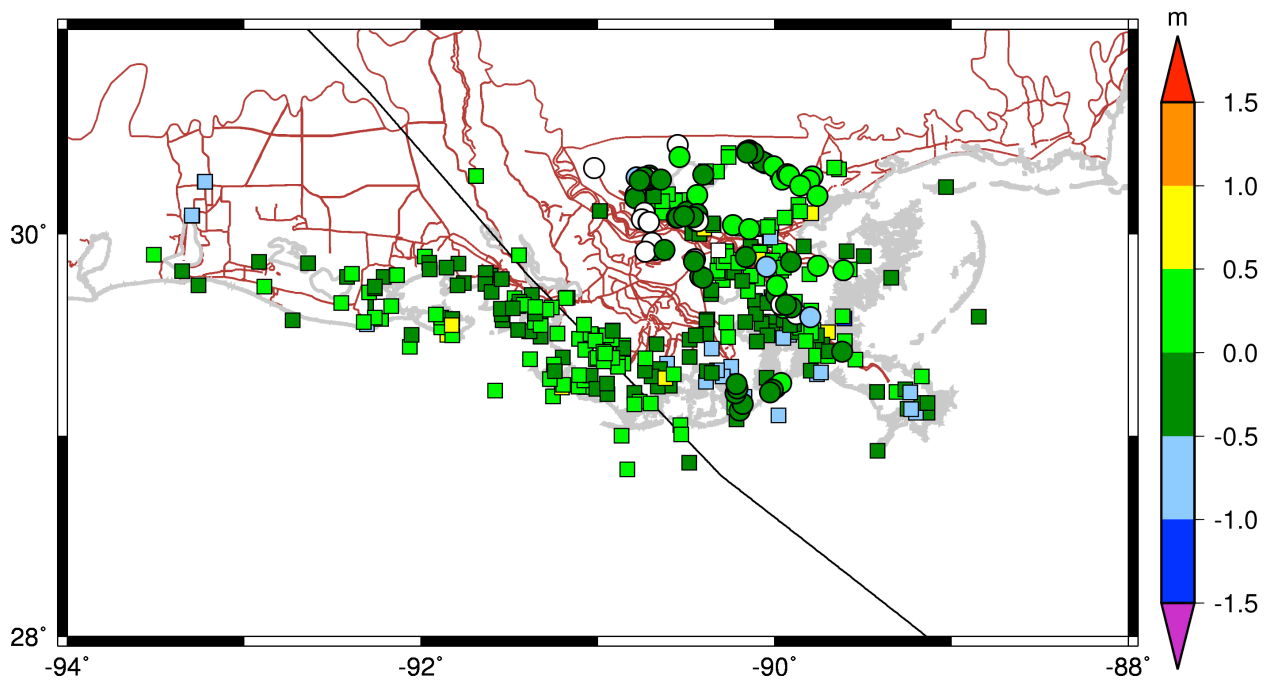


Figure 28: Locations of the 82 URS/FEMA HWMs (circles) and 362 hydrographs (squares) in southeastern Louisiana. The points are color-coded to show the errors (modeled less measured) between the peak water levels; green points indicate matches within 0.5m. Warm colors indicate locations where ADCIRC over-predicted the peak water level, while cool colors indicate locations where ADCIRC under-predicted the peak water level. White points indicate locations that were never wetted by ADCIRC.

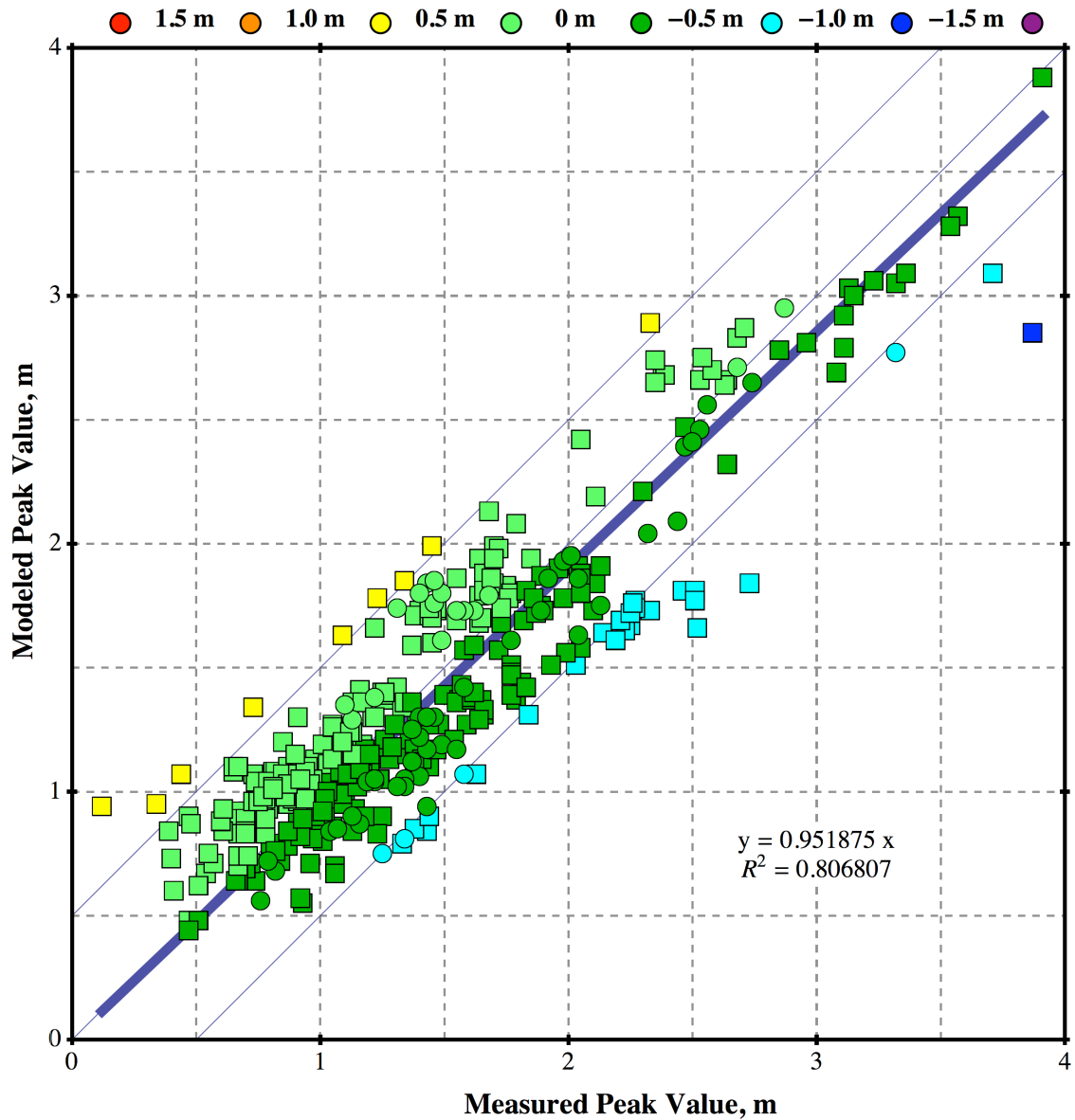


Figure 29: Scatterplot of FEMA HWMs (circles) and peak hydrograph water levels (squares) for Gustav. Green points indicate a match within 0.5m. Red, orange, yellow and light green circles indicate overprediction by the model; green, blue, dark blue and purple circles indicate underpredictions. The slope of the best-fit line through all points is 0.95 and the R^2 value is 0.81.

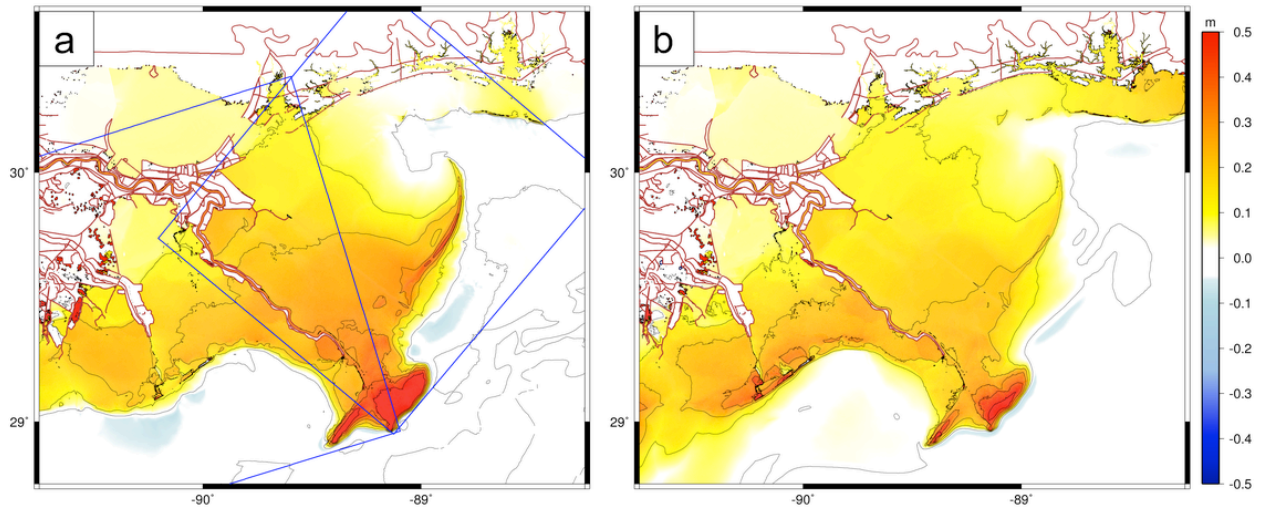


Figure 30: Maximum Gustav event wave-induced set-up produced by coupling ADCIRC to (a) STWAVE and (b) SWAN. The extents of the two structured STWAVE domains are shown in blue lines.